UCLA

UCLA Electronic Theses and Dissertations

Title

Effect of tamoxifen treatment on body temperature and bone regulation in mice

Permalink

https://escholarship.org/uc/item/7kd0892x

Author

PARK, JAE WHAN

Publication Date

2019

Peer reviewed|Thesis/dissertation

UNIVERSITY OF CALIFORNIA

Los Angeles

Effect of tamoxifen treatment on

body temperature and bone regulation in mice

A thesis submitted in partial satisfaction

of the requirements for the degree Master of Science

in Physiological Science

by

Jae Whan Park

ABSTRACT OF THE THESIS

Effect of tamoxifen treatment on

body temperature and bone regulation in mice

by

Jae Whan Park

Master of Science in Physiological Science

University of California, Los Angeles, 2019

Professor Stephanie M. Correa, Chair

As a selective estrogen receptor modulator, tamoxifen is known to act as estrogen receptor (ER) antagonist in ER positive cancer cells. Since many of the metabolic functions of estrogen are mediated by ERα in the hypothalamus, we hypothesized that tamoxifen affects body temperature and bone metabolism by modulating ERα signaling in the hypothalamus. To test this hypothesis, a genetic mice model that lacks ERα in the medial basal hypothalamus were used. These ERα knock-out mice and wild-type littermates were treated with either tamoxifen or vehicle for four weeks. Their body weight, core body temperature, tail skin temperature femoral bone length and density were measured. Tamoxifen treatment reduced core body temperature in wild-type but not ERα brain knock-out mice. On the other hand, tamoxifen increased bone mass in wild-type while it reduced bone mass when ERα is knocked out in the hypothalamus. These data indicate that tamoxifen could affect body temperature via ERα in the hypothalamus and bone density in different ways in the periphery versus the brain.

The thesis of Jae Whan Park is approved

Amy C. Rowat

Xia Yang

Stephanie M. Correa, Committee Chair

University of California, Los Angeles

2019

Dedication

To Dr. Stephanie Correa, deepest thanks for allowing me to join the lab and help me with everything that I struggled. The experience in Correa Lab changed my life. I can not explain in words how much I appreciate for everything.

To Dr. Zhi Zhang, I would not be able to find any better mentor, thank you for everything including teaching me so many things.

To my wife, Maria and my daughter, Eunice, without your support, this wouldn't be possible. Love you.

Table of contents

List of Figures

Background

Tamoxifen has been used for effective endocrine treatment of estrogen receptor positive breast cancers for more than 20 years (1). As a selective estrogen receptor modulator (SERM), tamoxifen can competitively antagonize estrogen receptors and reduce the proliferation of breast cancer cells. Clinical trials have shown that tamoxifen treatment reduces the incidence of contralateral breast cancer by as much as 40-50% and reduces recurrence for at least ten years of continuous treatment (2). Despite the stirring curative effect, tamoxifen treatment has been associated with increased risk of pulmonary embolism, deep vein thrombosis, endometrial cancer, hot flushes, and bone loss (3). Some of these negative side effects resemble menopausal symptoms in premenopausal women, including hot flushes and bone loss (13, 14). It remains unclear, however, how tamoxifen leads to these side effects. Thus, this study aims to distinguish the therapeutic effects from adverse effects. Specifically, we want to understand the effects of tamoxifen on body temperature regulation and bone metabolism through the brain.

It has been shown that Estrogen Receptor alpha (ERα) signaling in hypothalamus plays a key role in energy metabolism including feeding, thermogenesis and locomotor activity (4,5) Conditional knock-out (KO) of ERα in the steroidogenic factor 1 (*Sf1)* cell lineage in the ventromedial hypothalamus (VMH) led to a decline in thermogenesis while KO of ERα in the pro-opiomelanocortin (POMC) linage in the arcuate (ARC) resulted in higher food intake (6). Surprisingly, ERα in the hypothalamus also significantly regulates bone mass. In a mouse model where ERα is ablated in the *Nkx2-1* lineage (*Esr1 f/f; Nkx2-1Cre*), a gene largely expressed in the medial basal hypothalamus (MBH), the mice showed a dramatic increase of bone density compared to wild-type controls (7). In addition, ERα in the *Nkx2-1* lineage is also tightly linked with movement and heat production (4, 7). Therefore, we hypothesized that tamoxifen affects

1

temperature and bone density regulation by altering ERα signaling in the hypothalamus. To this end, we will use *Esr1 f/f; Nkx2-1Cre* mice model to test the effect of tamoxifen on core body temperature and bone mass with or without ERα in the hypothalamus. This study could reveal the role of hypothalamus in some of the side effects of tamoxifen treatment observed in breast cancer patients and help with developing new therapies that circumvent the side effects of tamoxifen.

Methods

-Mice

We crossed *Nkx2.1 Cre* mice with *Esr1* (ERα gene) floxed mice to generate knock-out mice (KO) have ERα knock-outs in the hypothalamus. Wild-type (WT) littermates (*Esr1 f/f;* no Cre) were selected as controls. Only female mice were used. Mice were 8 weeks old at the start of experiments. All mice were maintained under a 12:12 hour L/D schedule, and allowed to receive food and water unless otherwise indicated. Mice were at 8-10 weeks at the start of all the experiments.

All studies were carried out in accordance with the recommendations in the Guide for the Care and Use of Laboratory Animals of the National Institutes of Health. UCLA is AALAS accredited and the UCLA Institutional Animal Care and Use Committee (IACUC) approved all animal procedures.

-Group setup

We designed four groups according to different genotypes and treatments. See Figure 1(A). Briefly, there were two groups of conditional KO mice, one treated with tamoxifen and the other treated with vehicle. Additionally, there were two groups of *Esr1^{f/f}* controls, one treated with tamoxifen and the other treated with vehicle.

A

group	strain	treatment	n=42
WT-Veh	Esr1 fl/fl	Oil (Vehicle)	9
WT-Tax	No Cre	Tamoxifen(0.1mg/kg/d)	13
KO-Veh	Esr1 fl/fl	Oil (Vehicle)	9
KO-Tax	Nkx2-1Cre	Tamoxifen(0.1mg/kg/d)	11

B
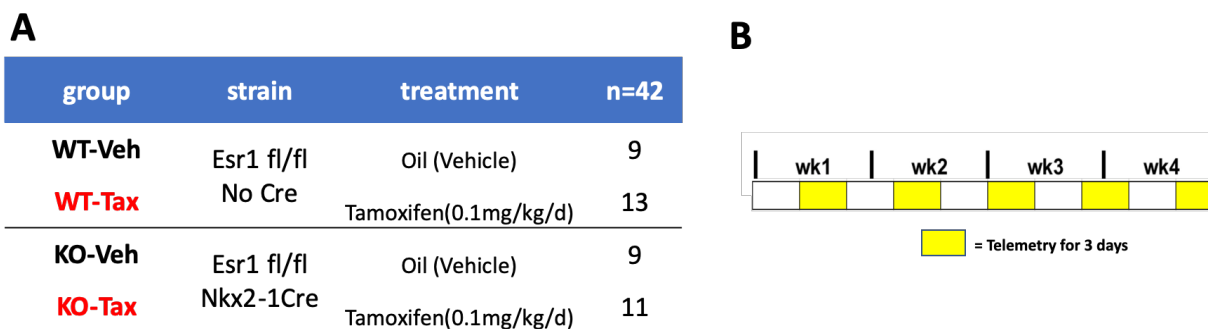
Figure 1. Experimental design. (A) Group set up with administration of tamoxifen or vehicle. **(B)** A schedule for telemetry measurement for core body temperature.

-Tamoxifen Administration

Tamoxifen (Sigma) was dissolved in corn oil at a concentration of 50 ug/ml. We performed daily injection of Tamoxifen for 0.1 mg/kg or equal amount corn oil (50ul) as vehicle for four weeks subcutaneously. We chose the dose based on previous experiment (8), where they found the change in bone mineral density with the injection for four weeks. We estimate that this dose models human tamoxifen exposure based on studies of tamoxifen in human serum, estimates of total blood volume in mice, and bioavailability of tamoxifen delivered via subcutaneous injection. (17) Additionally, it is on the low end of what is used effectively in previous studies (18,19), which is desirable to minimize off-target effects.

-Core Temperature and activity Measurement

A G2 eMitter (Starr Life Sciences) was implanted to the abdominal cavity and attached to the inside body wall of a mouse. Mice were single-housed in cages placed on top of ER4000 Energizer/Receivers. Nesting material was held constant to normalize behavioral temperature regulation. Gross movement and core body temperature were measured every 5 min using VitalView software (Starr Life Sciences). Tail skin temperature was monitored every 5 min using

a Nano-T temperature logger (Star-Oddi). The logger was attached to the ventral surface and 1 cm from the base of the tail in a 3D-printed polylactic acid collar

-Brown Adipose Tissue (BAT) measurement

Infrared thermal images were captured using Industrial camera VarioCAM® HD head 800 (InfraTec infrared LLC) before (t0) CNO or vehicle injection, then 10 min, 20 min, 30 min, 50 min, 120 min and 240 min after injection. The infrared images were analyzed using software IRBIS3 (InfraTec infrared LLC). BAT skin temperature was the average temperature of a circular region above interscapular BAT and tail skin temperature was the average temperature of a 1 cm line along the tail starting at 1 cm from the base of the tail

-In vivo bone analysis

At the end of the experiment, mice were perfused first with ice-cold PBS (pH 7.4) and then with 4% PFA with PBS. Femoral bones were collected and stored in PBS in -20°C. Whole femoral bones were scanned using Scanco Medical Micro-computed tomography (u-CT) scanner. For trabecular bone analysis, region of interest was selected at 1mm length proximal to the epiphyseal plate. A length of a femoral bone was also measured.

-RNA isolation and Real Time PCR (qPCR)

Total RNA from BAT was homogenized and isolated using ZymoRNA isolation kit (ZYMO Research) and RNA yield was determined using the NanoDrop D1000. cDNA synthesis was performed with equal RNA input using the Transcriptor First Strand cDNA synthesis kit. Quantitative PCR was performed using C1000 Touch Thermal Cycler and SYBR mix.

-Statistics

Data are represented as mean ± SEM. Data with normal distribution and similar variance were analyzed for statistical significance using two-tailed, unpaired Student's t-tests. Paired data were analyzed by paired t-tests. Comparisons for more than two groups were analyzed by one-way ANOVA followed by post-hoc Tukey's analysis. Significance was defined at a level of $P < 0.05$. Statistics were performed using GraphPad Prism 7/8.

Results

Body weight was recorded over four weeks and there were no significant changes in any of groups (Fig. 2A). Two Way ANOVA indicates KO mice show signifcant higher activity compared to WT and treatment of tamoxifen did not change activity signifantly. (Fig. 2B) There were no overall significant difference between four groups before injection, but after tamoxifen treatment there was significant temperature decrease in WT mice but not in KO mice. (Fig. 2C) Also the decrease in core body temperature in a daytime right after the injection was more significant compared to following night time in WT mice with tamoxifen injection (Fig. 2C). A decrease in core body temperature was also treatment. (Fig. 2D) However, in KO mice, tamoxifen did not alter core body temperature, suggesting that ERα signaling in hypothalamus is required for the effects of tamoxifen on temperature. (Fig. 2D) observed in WT mice in average of 24-hour data with tamoxifen
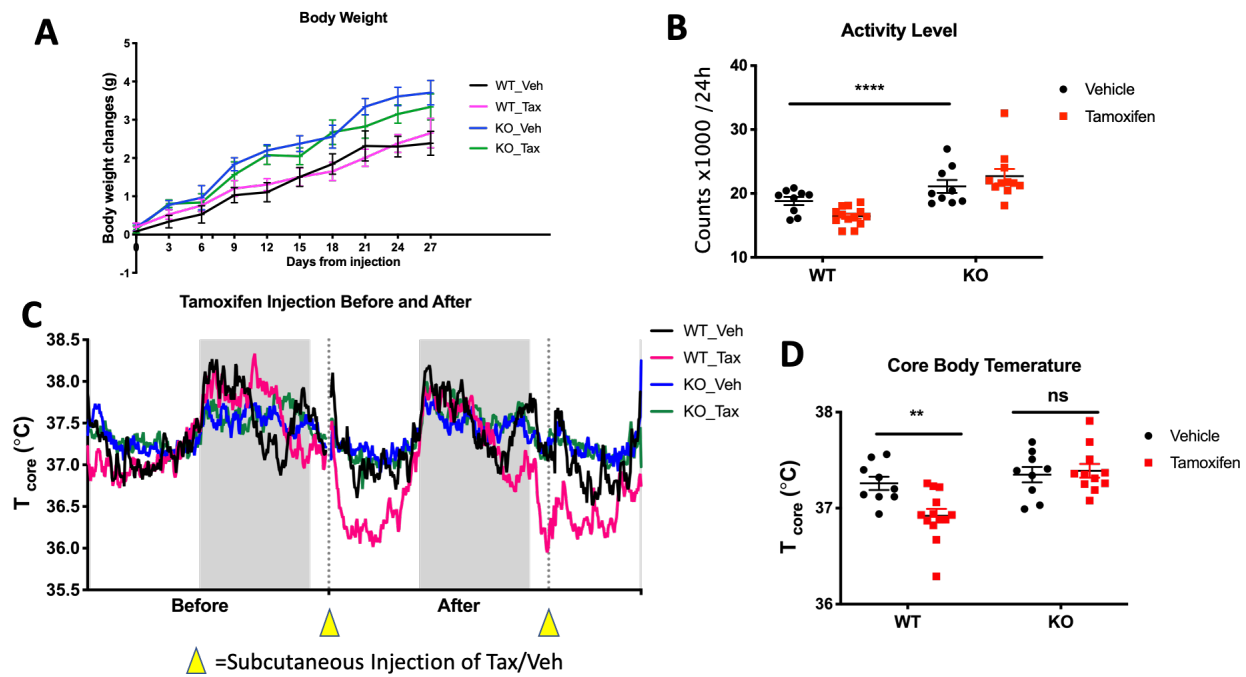
Figure 2. Effect of tamoxifen on body weight, activity level and core body temperature over four weeks of injection of tamoxifen or vehicle. (A) The changes in body weight were recorded over four weeks of injection. **(B)** Average 24 hours acitivity measured by any movement over four weeks. **(C)** 24 hours core body temperature of a day before and after tamoxifen or vehicle injection. White colored area indicates day time and gray area indicates night time, n=6-10 per group. Yellow arrow indicates an injectoin of either tamoxifen or vehicle. **(D)** Average over 24 hours of core body temperature after four weeks of injection of tamoxifen or vehicle.

In order to determine change in core temperature is from whether in heat production from BAT or heat dissipation from tail, we measured BAT and tail skin temperature. KO mice had significantly higher tail skin temperature compared to WT, indicating that there is more vasodilation. (Fig. 3A) Tamoxifen treatment decreased in temperature in KO mice, which was also significantly different. (Fig. 3A) To better visualise heat dissipation, we introduced Heat Loss Index (HLI), which was

calculated from follwing equation, HLI = (Tskin − Tambient) / (Tcore − Tambient) (15) (Fig. 3B)

There is a significant differences between WT mice and KO mice in vehicle treatment and

tamoxifen treatment decreased heat dissipitation in KO mice. (Fig. 3B) There is also a trend that

tamoxifen treatment in WT mice had higher dissipitation, but not statstically significant. (Fig. 3B)

There was no significant differences in temperature in BAT, but there is an indication tamoxifen
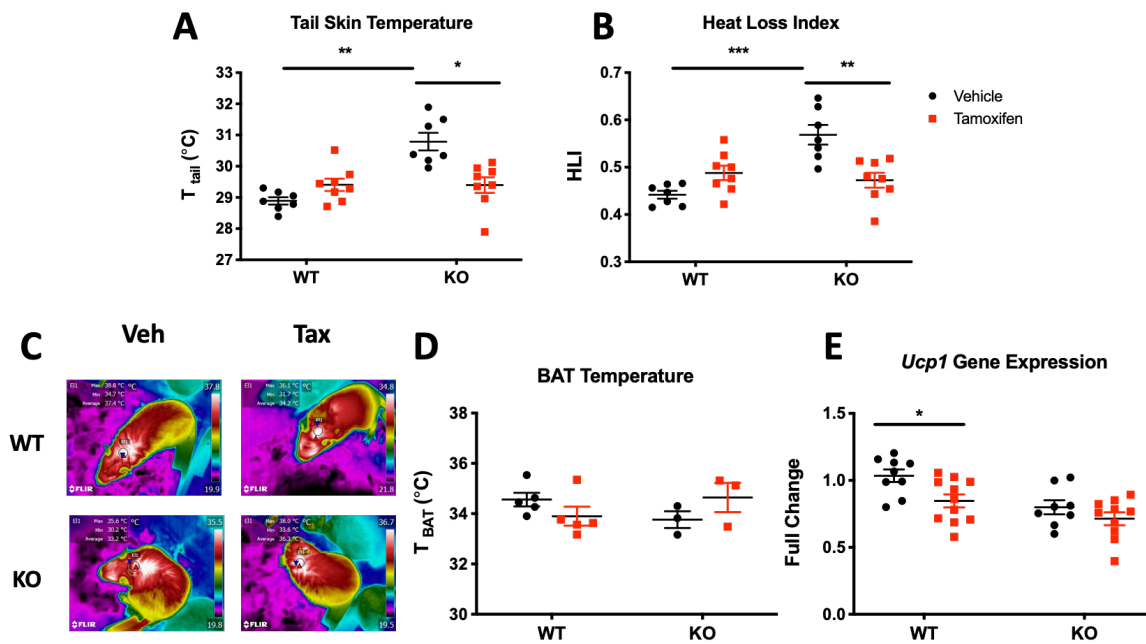
Figure 3. Effect of tamoxifen on Brown Adipose Tissue (BAT) and tail skin temperature after four weeks of injection of tamoxifen or vehicle. (A) Measurement of tail skin temperature using temperature probes attached to the tail skin. **(B)** Heat dissipation indicated by Heat Loss Index (HLI) [Vasoconstriction = 0, Vasodilation =1]. **(C)** Representative images from thermal imaging, with region of interest in the area above the BAT. **(D)** Quantitation of thermal camera images above the BAT. **(E)** A relative expression of *Ucp1* transcripts in BAT as measured by qPCR.

treatment decreased the temperature in WT mice, not in KO mice. (Fig. 3C, 3D) More quantitative

analyses are underway to determine if these effects are statistically significant with more sample

sizes. Ucp1 gene expression, which is a marker for BAT thermogenesis was measured by qPCR

(16) (Fig. 3E) Tamoxifen treatment decreased Ucp1 gene expression in WT mice, not in KO mice,

suggesting lower heat production from BAT with tamoxifen treatment. (Fig. 3E)

Figure 4. Effects of tamoxifen on bone volume and length. **(A)** Representative images

from Micro-CT scan showing bone tissue in both wild type and KO mice after four weeks of

treatment with tamoxifen or vehicle. **(B)** Fractional bone volume measured in trabecular

bone by dividing bone volume (BV) divided by total volume (TV). **(C)** Measurement of

femoral bone length in millimeters (mm).

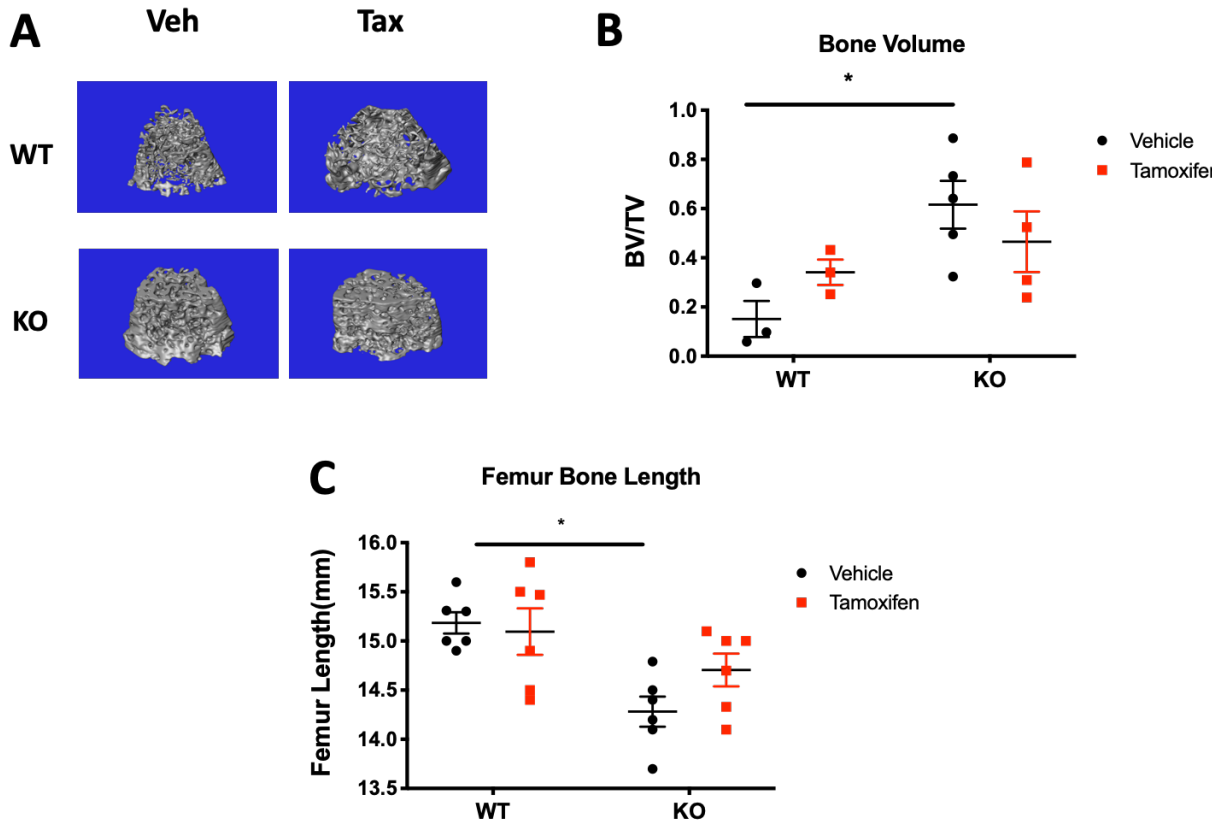After four weeks of daily injection, femoral bone samples were collected. Vehicle-treated KO mice appear to have higher bone density compared to vehicle-treated WT mice (Fig. 4A, 4B). Although the samples sizes are small, preliminary analyses suggest that tamoxifen treatment may increase bone density in WT mice (Fig.4B). In contrast, tamoxifen treatment may decrease bone density in KO mice compared to KO mice with vehicle treatment (Fig. 4B). More quantitative analyses are underway to determine if these effects are statistically significant. Analyses of femoral bone length indicate that bone length is shorter in KO mice compared to WT mice, but the effects of tamoxifen compared to vehicle appear similar both the WT or KO groups (Fig. 4C).

Discussion

Our study aimed to understand how tamoxifen affects temperature and bone, two tissues that are modulated by tamoxifen in breast cancer patients receiving tamoxifen treatment. Because tamoxifen is associated with side effects of hot flushes, in which people experience excessive sudden of heat dissipation responses (10), we tested whether tamoxifen can alter body temperature in mice. Indeed, tamoxifen treatment decreased core body temperature in wild-type mice. Because body temperature is maintained by a balance between heat production and dissipation, the observed decrease in core body temperature could be partly due to an increase in heat dissipation, which is in line with the etiology of hot flushes as seen in patients receiving tamoxifen. Indeed, we find that tamoxifen alters heat dissipation differently in WT and KO mice. However, we were unable to detect a significant effect of tamoxifen on tail temperature or HLI (Fig. 3A, B). Thus, the tamoxifen-induced drop in core temperature that is observed in WT mice may be due largely to a significant reduction in thermogenesis by the BAT (Fig. 3E).

Recent studies have shown that estrogen signaling in the hypothalamus regulates thermogenesis in female mice and rats (4,5). Interestingly, our data showed that tamoxifen

decreased body temperature only in WT mice, but not in mice absent of ERα in hypothalamus. These effects are probably mediated by ERα from the brain because the ERα brain knockout mice exhibited no changes in core body temperature with tamoxifen treatment. These results suggest that tamoxifen may regulate core body temperature through ERα in the hypothalamus. Also, the tamoxifen-induced changes in body temperature cannot be attributed to hyperactivity or changes in basal metabolic rate, as there were no changes in body weight or activity levels.

Elevations in tail skin temperature are associated with heat dissipation. KO mice had higher skin temperature compared to WT, suggesting that KO mice may have higher heat dissipation in general. Tamoxifen treatment significantly decreased the heat dissipation in KO mice but not in WT littermates. Also, Heat Loss Index (HLI), which indicates vasoconstriction or vasodilation, was higher in KO mice and decreased by tamoxifen treatment. Both data from tail skin temperature and HLI show higher heat dissipation in mice in absence of ERα in the hypothalamus. Further studies are required to determine if the effects of tamoxifen on heat dissipation are mediated by other estrogen receptors, other areas of the brain, or other estrogen-sensitive tissues.

Brown Adipose Tissue (BAT) generates heat to regulate body temperature. We investigated BAT temperature with thermal (infrared) imaging, but due to insufficient sample sizes, this data are inconclusive. However, when analyzing expression of the *Ucp1* transcript, which is associated with BAT activity (16), *Ucp1* was lower in WT mice with tamoxifen treatment. Thus the tamoxifen-induced drop in core temperature may be largely due to a decrease in heat production by the BAT.

Although estrogen signaling is known to be generally beneficial for bone mineral density (11), the effect of estrogen signaling in the brain goes in opposite direction. Depletion of in ERα in the hypothalamus increases bone density even when ovarian hormones were removed (7). Although tamoxifen has been used in treatment of osteoporosis in women after menopause, the effect of tamoxifen on bone, however, may depend on estrogen status. A clinical report showed

tamoxifen actually decreased bone mass in premenopausal women (12). Our preliminary analyses suggest that there may be an increase in bone density with tamoxifen treatment in wild type mice. As previously shown (7), our data confirm that vehicle-treated ERα knockout mice appear to have higher bone density compared to vehicle-treated WT mice. Tamoxifen treatment showed trends toward increase in bone density in WT mice, but tended to decrease bone density in mice with ERα KO in hypothalamus. This suggests that tamoxifen might act to increase bone density through ERα in hypothalamus, but decrease the bone density from the outside of the hypothalamus. More samples will be added in future to adequately test this hypothesis. However, the potential increase in bone volume following tamoxifen treatment suggests that we were unable to model the side effect of bone loss in our studies.

Although it is still unclear the precise pathways by which tamoxifen affects body temperature or bone, our results indicate that tamoxifen has modulatory effects on ERα signaling in hypothalamus plays. Thus, the effects of tamoxifen on the hypothalamus may play a critical role in the known adverse effects during tamoxifen treatment, particularly for temperature regulation and hot flashes. Ultimately, these studies could help to develop better therapy for breast cancer treatment while bypassing the some of the adverse side that might interfere with treatment or reduce quality of life in breast cancer patients and survivors.

References

1. G. L. Gierach, R. E. Curtis, R. M. Pfeiffer et al., Association of Adjuvant Tamoxifen and Aromatase Inhibitor Therapy With Contralateral Breast Cancer Risk Among US Women With Breast Cancer in a General Community Setting. JAMA Oncol, (2016).

2. J.Chang, T.J.Powles, D.C. Allred et al., Prediction of Clinical Outcome from Primary Tamoxifen by Expression of Biologic Markers in Breast Cancer Patients. Clin Cancer, (2000)

3. S Cykert, N Phifer, Hansen C et al., Tamoxifen for breast cancer prevention: a framework for clinical decisions. Obstet Gynecol (2004)

4. S. Correa, D.W.Newstrom et al., An Estrogen-Responsive Module in the Ventromedial Hypothalamus Selectively Drives Sex-Specific Activity in Females. Cell Reports (2015)

5. Y. Xu, T.P.Nedungadi et al., Distinct Hypothalamic Neurons Mediate Estrogenic Effects on Energy Homeostasis and Reproduction. Cell Metab. (2015)

6. Xu, Y. et al. Distinct hypothalamic neurons mediate estrogenic effects on energy homeostasis and reproduction. Cell metabolism 14, 453–65 (2011).

7. Herber, C. B. et al. Estrogen signaling in arcuate Kiss1 neurons suppresses a sex dependent female circuit promoting dense strong bones. Nature Communications 10,163 (2019).

8. M.J.Perry et al., Tamoxifen Stimulates Cancellous Bone Formation in Long Bones of Female Mice. Endocrinology (2015)

9. P.B.M. de Morentin et al., Estradiol Regulates Brown Adipose Tissue Thermogenesis via Hypothalamic AMPK. Cell Metab. (2014)

10. J.E.Mortimer et al., Tamoxifen, hot flashes and recurrence in breast cancer. Breast Cancer Res Treat. (2009)

11. Imai Y et al., Estrogens maintain bone mass by regulating expression of genes controlling function and life span in mature osteoclasts. AANY Acad Sci. (2009)

12. L. Vehmanen et al., Tamoxifen treatment after adjuvant chemotherapy has opposite effects on bone mineral density in premenopausal patients depending on menstrual status. J Clin Oncol. (2006)

13. P. Tuomikoski et al., Menopausal hot flushes and vascular health, Annals of Medicine. (2011)

14. R. Lindsay, The menopause and osteoporosis, Obstetrics & Gynecology. (1996)

15. Romanovsky, A.A., A.I. Ivanov, and Y.P. Shimansky, Selected contribution: ambient temperature for experiments in rats: a new method for determining the zone of thermal neutrality. J Appl Physiol (1985)

16. Kristy L. Townsend, Yu-Hua Tseng, Brown fat fuel utilization and thermogenesis, Trends in Endocrinology & Metabolism, (2014)

17. Slee, P. H., De Vos, D., Chapman, D. & Stevenson, D. The bioavailability of Tamoplex (tamoxifen). *Pharm Weekbl Sci* 10, (1988)

18. Wang, Q., Jiang, J., Ying, G., Xie, X.-Q., Zhang, X., Xu, W., Zhang, X., Song, E., Bu, H., Ping, Y.-F., Yao, X.-H., Wang, B., Xu, S., Yan, Z.-X., Tai, Y., Hu, B., Qi, X., Wang, Y.-X., He, Z.-C., Wang, Y., Wang, J. M., Cui, Y.-H., Chen, F., Meng, K., Wang, Z. & Bian, X.-W. Tamoxifen enhances stemness and promotes metastasis of ERα36+ breast cancer by upregulating ALDH1A1 in cancer cells. *Cell Research* **28,** 336 (2018).

19. Perry, M. J., Gujra, S., Whitworth, T. & Tobias, J. H. Tamoxifen stimulates cancellous bone formation in long bones of female mice. *Endocrinology* **146,** 1060–5 (2005).

Appendix: Single cell profiling of the VMH reveals a sexually dimorphic regulatory node of energy expenditure

J. Edward van Veen[1,2,7], Laura G. Kammel[1,2,3,7], Patricia C. Bunda[1], Michael Shum[4,6], Michelle S. Reid[1], Jae W. Park[1], Zhi Zhang[1, 2], Megan G. Massa[1, 2, 5], Douglas Arneson[1], Haley Hrncir[1], Marc Liesa[4,6], Arthur P. Arnold[1,2], Xia Yang[1], and Stephanie M. Correa[1,2]

Affiliations:

[1] Department of Integrative Biology and Physiology

[2] Laboratory of Neuroendocrinology of the Brain Research Institute

[3] Molecular, Cellular, and Integrative Physiology Graduate Program

[4] Division of Endocrinology, Department of Medicine, and Department of Molecular and Medical Pharmacology, David Geffen School of Medicine

[5] Neuroscience Interdepartmental Doctoral Program

[6] Molecular Biology Institute,

University of California, Los Angeles, CA, USA

[7] authors contributed equally

author for correspondence: stephaniecorrea@ucla.edu

Statement of contribution

Thermogenesis and physical activity are modulated by estrogen receptor alpha (ERα) signaling in the sexually dimorphic ventromedial nucleus of the hypothalamus (VMH), but the precise neuronal populations involved remain undefined. In the following study, we use single cell transcriptomics to identify diverging neuronal populations in the mouse VMH, three of which show sex biased gene expression in adults. In females, ER expression is restricted to two intermingled populations: tachykinin 1 (*Tac1*)-expressing neurons that promote physical activity and previously uncharacterized reprimo (*Rprm*)-expressing neurons. Despite sex differences within ERα$^+$ VMH neurons, chemogenetic activation similarly increases movement and heat generation in both sexes. However, silencing *Rprm* gene function increases core temperature, but not movement, selectively in females. Together, our results suggest that developmental estrogen signaling induces permanent changes in specialized neuron populations of the VMH that underlie established sexually dimorphic metabolic phenotypes. These studies were led by Ed van Veen, PhD and Laura Kammel, PhD who contributed equally and are listed as co-first authors. My contribution was to help optimize the dissociation protocol that we used to collect VMH neurons from mouse pups, to cut brain sections for spatial gene expression analysis, and perform immunohistochemistry to localize ERa and pMEK immunoreactivity in Figure S1. Additionally, I performed other studies that are not included in the submitted manuscript due to the absence of significant effects, such as qPCR analysis of thermogenic gene expression in brown adipose tissue from the animals included in Figure 6.

Abstract

Estrogen signaling in the central nervous system promotes weight loss by increasing thermogenesis and physical activity in the ventromedial hypothalamus (VMH), but the precise neuronal populations regulating these aspects of energy expenditure remain unclear. Here we define the molecular and functional heterogeneity of the VMH using single cell RNA sequencing, *in situ* hybridization, chemogenetic activation, and targeted gene knockdown. We describe six molecularly distinct neuron clusters in the VMH. In females, estrogen receptor alpha (ERα) is restricted to neurons expressing tachykinin-1 (*Tac1*) or reprimo (*Rprm*). Further, *Tac1* and *Rprm* expression is enriched in females, a sex difference that is established by permanent effects of gonadal hormones early in life. Finally, while *Tac1* ablation selectively impairs movement, here we show that silencing *Rprm* selectively dysregulates temperature without affecting physical activity. Together this work provides a novel architectural framework whereby distinct and sexually differentiated neuron populations within the VMH mediate sex-specific aspects of metabolic homeostasis.

Introduction

Women transitioning to menopause exhibit decreased energy expenditure and decreased fat oxidation compared to age-matched premenopausal women[1]. Similar to humans, rodents exhibit estrogen-induced changes in energy expenditure; female rats exhibit cyclic patterns of wheel running throughout the estrous cycle[2,3] and female mice exhibit similar cyclicity in temperature and locomotion[4–6]. These effects are mediated by estrogen receptor alpha (ERα) signaling: eliminating ERα either globally or in the central nervous system leads to obesity due increased feeding, reduced movement, and reduced thermogenesis[7–9]. While estrogen-based hormone therapy can improve metabolic profiles after menopause, it is associated with higher cardiovascular disease risk[10] and, in the case of estrogen plus progestogen therapy, higher breast cancer risk[11]. To ultimately circumvent the risks associated with systemic estrogen therapy, we aim to pinpoint neurons that control systemic energetic balance and define their responses to estrogen signaling.

Recent work has begun to define the neuron populations that mediate the effects of ERα signaling on energy balance. Conditional knockout mouse models suggest that ERα signaling modulates feeding in female mice via neurons of the pro-opiomelanocortin (*Pomc*) lineage, possibly located in the arcuate nucleus (ARC)[5,9,12,13] or outside the medial basal hypothalamus[14]. Additionally, ERα signaling modulates two types of energy expenditure, spontaneous physical activity and thermogenesis, via neurons of the steroidogenic factor 1 (*Sf1/Nr5a1*) lineage in the ventromedial hypothalamus (VMH)[9,15–17]. However, ERα-expressing neurons of the VMH have many functions. In addition to female-specific roles in energy expenditure, ERα^{+} VMH neurons control fear, territorial aggression, and self defense in males, maternal aggression in females, and mating behaviors in both sexes[18–23]. We hypothesize that these diverse and sex-specific functions are mediated by distinct subpopulations of ERα^{+} neurons. Consistent with this notion, distinct neuronal ensembles are activated in the ventrolateral region of the VMH (VMHvl) of male mice

during interactions with male or female conspecifics[18,24]. While these neuron populations remain to be defined, a subset of ERα^{+} neurons in the VMH, which co-express tachykinin 1 (*Tac1*) and oxytocin receptor (*Oxtr*), drive estrogen-dependent changes in physical activity in females[17,25]. However, the VMHvl populations that control other sex-specific behaviors, such as estrogen-dependent increases in thermogenesis, have not been identified.

The VMH is sexually dimorphic with respect to hormone responsiveness, gene expression, neurochemistry, synaptic organization, and neuron function[26–28]. Here, we use RNA sequencing with single cell resolution to test the hypothesis that neurons in this region are heterogenous and sexually dimorphic. We define six major neuron populations in the VMH and a new sexually dimorphic transcript in the VMHvl, reprimo (*Rprm)*, which regulates core body temperature. Collectively, these studies demonstrate that estrogen regulates energy expenditure in females through two intermingled but distinct neuronal subsets, and suggest that the VMH serves as a hormone-responsive nexus of distinct neural circuits controlling metabolic homeostasis.

RESULTS

Single Cell Transcriptomics Reveals Neuronal Heterogeneity in the VMH

We used a fluorescent reporter strategy to isolate neurons of the VMH and single cell RNA sequencing to cluster neurons by transcriptional signature. To selectively label VMH neurons, the *Sf1Cre* driver[29] was crossed to mice carrying a latent allele of tdTomato *(Ai14)*[30] (Figure 1a). Importantly, this strategy yields tdTomato expression in neurons of the entire VMH upon Cre expression, including in the ventrolateral VMH where it overlaps with ERα immunoreactivity in both males and females (Figure 1b, c) as in [31]. tdTomato expression in surrounding hypothalamic regions, the dorsomedial hypothalamus (DMH) and the arcuate nucleus (ARC), was detectable but scattered and infrequent (Figure 1b, c, white arrowheads). Fluorescence aided cell sorting

(FACS) was performed on single cell suspensions of hypothalami to isolate live neurons of the *Sf1* lineage for single cell transcriptomic analysis (Figure 1d).

Unicellular transcriptional analysis of 530 single cells from 3 male and 3 female postnatal day (P) 10 mice detected an average (median) of 2556 genes per single cell and revealed strong and consistent expression of the neuronal markers β3-tubulin (*Tubb3*) and neurofilament light peptide (*Nefl*), while very few cells exhibited detectable expression of the glial markers *Gfap* and *Olig1* (Figure 2a). Consistent with the VMH being predominantly glutamatergic, high expression of the glutamatergic marker *Slc17a2* and consistently low expression of the GABAergic marker *Gad2* was observed in all samples (Figure 2a). Finally, to assess how dissociation and FACS sorting may have affected gene expression, we examined immediate early gene expression. Expression of *Fos* and *Arc*, used as a readout for isolation stress and activation[32,33], appears undetectable in the majority of cells from suspensions obtained from different animals and sexes (Figure 2a). Overall, we conclude that the *Sf1Cre*-mediated fluorescent reporter strategy primarily yields healthy VMH glutamatergic neurons.

To determine if VMH neurons show heterogeneity in gene expression profiles, we used a Shared Nearest Neighbor (SNN) algorithm to identify clusters comprised of transcriptionally similar cells[34]. A uniform manifold approximation and projection (UMAP) revealed a main cluster and two divergent clusters (Figure 2b). Within the main cluster, UMAP-based separation was less pronounced, as may be expected when examining neurons of a single transcription factor lineage (*Sf1Cre*). Nevertheless, we detected distinct clusters marked by differential expression of genes that have known and unknown significance in the VMH. We identified a total of eight clusters, hereby identified by the top most differentially expressed transcript within each cluster (Figure 2b, c): *Tac1*, which has been previously demonstrated to promote physical activity in female mice[17]; reprimo (*Rprm*), a TP53 and ERα regulated gene[35] with no described role in the brain; prodynorphin (*Pdyn*), a gene encoding an endogenous opioid precursor with described roles in leptin-regulated energy homeostasis throughout the hypothalamus[36]; somatostatin (*Sst*), a

neuropeptide precursor gene which has hypothalamic roles in the negative regulation of growth hormone axis[37] and feeding[38]; hippocalcin-like protein 1 (*Hpcal1*) encoding a neuron-specific calcium binding protein; and galanin (*Gal*), a neuropeptide precursor gene shown to increase food consumption when injected into the VMH of rats[39]. In addition to the subpopulations in the principal six clusters, we identified two divergent clusters (Figure 2b, c): a cluster marked by differential expression of proopiomelanocortin (*Pomc*) and many other markers indicating an ARC derived origin, and one marked by differential expression of apolipoprotein E (*Apoe*) and many other markers of glial-like signature.

Comparing overall transcriptional signatures amongst the eight clusters (Figure 2d), the most divergent population are the cells with glial-like signature (*Apoe*+), followed by neurons expected to be from the ARC (*Pomc*). Neuron clusters expected to arise from the VMH are more closely related in overall expression signature. Remarkably, the expression of cluster-defining markers appears largely mutually exclusive (Figure 2e), suggesting distinct molecular signatures among neuron clusters of the VMH.

All the neuron clusters identified in the unicellular analysis of the VMH were obtained by analyzing males and females together (Supplementary Figure 1a). We then compared the gene expression profiles between males and females to determine whether sex-specific signatures existed in VMH neurons. The paternally-expressed gene necdin (*Ndn*) had the highest enrichment in males, whereas the proto-oncogene *Araf* had the highest enrichment in females (Supplementary Figure 1b). *Ndn* expression was consistently higher across all clusters in males (Supplementary Figure 1c) and RNA *in situ* hybridization (ISH) confirmed enrichment of *Ndn* transcripts in the male VMH as compared to females (Supplementary Figure 1d). *Araf* expression was detected to be consistently higher in neurons from females across clusters, compared to those from males (Supplementary Figure 1e). ISH of *Araf* was unable to clearly confirm the female biased expression in the VMH, though it appears that *Araf* expression in females might be slightly higher in the VMHvl (Supplementary Figure 1c, d). As *Araf* is a direct effector of the

RAF/MEK/ERK MAPK cascade, we sought to determine if this pathway is activated differentially in females. Intriguingly, we found female-specific phosphorylation of MEK in the VMHvl that co-localizes with ERα (Supplementary Figure 1g). This result supports a female specific role of MAPK signaling in the VMHvl as well as *Araf* as a target to be explored to induce changes in energy balance.

Sex differences established by gonadal hormones

To test the prediction that each neuron cluster generated by gene expression would have a correspondingly distinct spatial distribution within the intact VMH, we detected and localized the expression of the cluster-defining markers using ISH. Further confirming the efficiency of VMH neuron isolation used in the scRNA-seq, expression of all marker genes except *Pomc* was detected within the anatomical boundaries of the VMH (Figure 3 and Supplementary Figure 2a-d). The most restricted expression patterns were observed with *Tac1*, *Rprm*, *Pdyn,* and *Sst* (Supplementary Figure 2a-e). Analysis along the rostral-caudal axis revealed sexually dimorphic expression of *Tac1*, *Rprm*, and *Pdyn* in the caudal VMHvl (Figure 3a-c). Specifically, *Tac1* and *Rprm* expression were both significantly enriched in females within the caudal VMHvl (Figure 3a, b). In contrast, *Pdyn* expression was significantly enriched in males within the caudal VMHvl, although both males and females showed robust expression of *Pdyn* in the dorsomedial VMH (Figure 3c). Finally, we did not detect any major differences in expression of *Sst* between males and females (Figure 3d).

Sex hormones mediate permanent (organizational) differentiating effects on the brain during development, as well as reversible (activational) effects during adulthood, with additional contributions to sex differences caused by sex chromosome genes expressed within brain cells. To delineate how sexually dimorphic expression of cluster markers develops in the VMHvl, we used the four-core genotypes model[40] to reveal i) organizational effects of hormones, by comparing XX female vs. XX male or XY male vs. XY female, all gonadectomized (GDX) upon

22

sexual maturity, ii) activational effects of hormones, by comparing GDX vs. intact XX females or XY males, and iii) the effects of sex chromosomes, by comparing XX female vs. XY female or XX male vs. XY male, all GDX, as illustrated in Figure 4a. Expression patterns of both *Tac1* and *Rprm* were unchanged by GDX in females, showing that hormonal activation is not essential for dimorphic expression. Moreover, the presence of the Y chromosome in females did not change *Tac1* or *Rprm* expression, suggesting that the Y chromosome did not have a repressive role on these genes. However, gonadal sex was critical for determining these sexually dimorphic expression patterns, suggesting that these patterns are established during development and are maintained in adulthood (Figure 4b, c). In contrast, the expression pattern of *Pdyn* was distinct between GDX or intact females and gonad-intact males, but not GDX males (Figure 4d, Supplementary Figure 3), suggesting that *Pdyn* expression is maintained by differences in testicular sex hormone signaling in adulthood. Finally, we did not observe any sex differences in *Sst* along any of the three phenotypic comparisons (Figure 4e).

Two major estrogen-sensitive populations in the female VMHvl

Estradiol, as a metabolite of testosterone from the testes, plays a major role in the early permanent masculinization of the mammalian brain in males and the expression of male-specific behaviors To determine if any of the organizational and activational effects of sex hormones on neuronal cluster markers, specifically *Tac1*, *Rprm*, and *Pdyn*, could be related to estradiol action on ERα we first examined the expression of ERα by fluorescent ISH (FISH) within each cluster. In females, ERα immunoreactivity was robust in *Tac1*$^+$ cells and *Rprm*$^+$ cells (Figure 5a, b), but weak in *Sst*$^+$ cells (Supplementary Figure 4a). In males, we found that *Pdyn* expression co-localized with ERα immunoreactivity, despite lower ERα expression at both the transcript and protein levels compared to females (Figure 5c,d and Supplementary Figure 3c). We then investigated the spatial relationship of these ERα$^+$ neuron populations in females. *Tac1*$^+$ and *Rprm*$^+$ cells were highly intermingled within the VMHvl (Figure 5e), but largely spatially distinct

from *Sst*^{+} cells (Supplementary Figure 4b, c).

Finally, we asked if ERα is required for the sexually dimorphic expression of *Rprm* in females, as previous studies showed that *Tac1* expression was independent of ERα status in the VMHvl. We compared mice with genetic ablation of ERα in the *Sf1* lineage, which results in a substantial loss of ERα^{+} cells in the VMH[9], and a second mouse model lacking ERα in the *Nkx2-1* lineage, which shows near complete elimination of ERα both in the VMH and ARC[17]. Interestingly, we found that *Rprm* expression, similar to *Tac1* expression, was insensitive to ERα ablation in the female VMHvl (Figure 5f, g). Together, these findings are in line with evidence that early brain masculinization, rather than feminization, is dependent on estradiol-induced regulation of gene expression.

VMH Expression of Reprimo Regulates the Central Control of Temperature

To discern the role of ERα^{+} VMHvl neurons in energy expenditure, we first chemogenetically activated ERα neurons using the Cre-dependent DREADD (AAV-DIO-hM3Dq[41]) delivered bilaterally to the VMHvl of *Esr1Cre* knockin mice[20]. Administration of the DREADD ligand, clozapine-N-oxide (CNO), elicited a sustained (6 hour) increase in both heat and physical activity in *Esr1Cre* females compared to saline administration in the same mice on a different day and compared to CNO administration to wild-type littermates (Figure 6a, b and Supplementary Figure 5).

Previous studies suggest that *Tac1*^{+} neurons mediate estrogenic effects on physical activity but not thermogenesis, and that these neurons require *Tac1* expression to fully induce movement[17]. The neuronal population controlling thermogenesis in a sexual dimorphic manner, however, was still elusive. Thus, we hypothesized that the specific role of these newly identified *Rprm*^{+} neurons was to control thermogenesis. To test this hypothesis, we silenced *Rprm* gene function within the VMHvl using cell permeable siRNA pools delivered via bilateral stereotaxic injections (Figure 7a). When compared to animals injected with a non-targeting siRNA, the

animals injected with *Rprm* targeting siRNA showed a significant increase in body temperature (Figure 7b, c). The increase in temperature was persistent across time points (Figure 7b) and was significant both in the active night phase and the inactive day phase (Figure 7c). Importantly, *Rprm* knockdown did not induce changes in physical activity (Figure 7d), further supporting the notion that *Tac1*$^+$ neuronal function does not overlap with *Rprm*$^+$ neuronal function. These data demonstrate for the first time that there are at least two classes of ERα$^+$ neurons in the VMHvl that are functionally distinct, and together coordinate the female specific effects on physical activity and thermogenesis of this hormone-responsive region.

DISCUSSION

This study used the power of single cell RNA sequencing as a starting point for a high resolution atlas of the VMH, one of the brain's longest known sexually dimorphic regions. By performing our sequencing ten days after birth, we were able to discover populations established in development, before they are altered by hormonal changes associated with experience or puberty. Extensive validation experiments confirm all of the populations identified by sequencing analysis. Additionally, *in situ* hybridization comparing the sexes revealed novel sexually dimorphic populations in the caudal VMHvl that scRNA sequencing did not resolve. We detected only scattered reads from *Esr1* in our sequencing, but combining immunohistochemistry with in situ hybridization clearly identified specific populations that overlap with ERα expression, notably including the sexually dimorphic subpopulations of the VMH. Finally, *in vivo* validation experiments confirm that ERα⁺ neurons in the VMHvl play unique roles in regulating energy expenditure in females, and extend this finding by functionally and molecularly subdividing these neurons. Functional dissection of sex differences in the neural circuits that control food intake and energy expenditure is critical to understanding the biological basis of gender differences in the control of body weight.

Single cell RNA sequencing has led to dramatic improvements in understanding diverse cell populations of the hypothalamus, using dissociated brain tissue without purification of cell types [42,43]. Here, we extend these studies by using mice harboring a genetically encoded fluorescent lineage tracer (*Sf1-Cre; Ai14*). This approach was tailored to allow specific purification of VMH neurons by FACS prior to scRNA-Seq. We identified six major and two minor clusters of cells with distinct transcriptional signatures. Notably, previous studies do not identify the two clusters marked *Hpcal1* or *Rprm*, nor do they assign *Tac1*, *Pdyn*, *Sst,* or *Gal* populations to the VMH [42,43]. In contrast, targeted profiling of the *Sf1* lineage allows the study of the VMH with unprecedented resolution.

As the overall anatomy of the VMH is conserved between males and females (Figure 1b-c, 2b, Supplementary Figure 1a), it is curious how activation of equivalent neurons can evoke sex specific behaviors. It is now generally accepted that sexually dimorphic behaviors are sexually differentiated by sex hormones during critical developmental periods (reviewed in [44,45]). Estrogen signaling in the VMH has clearly demonstrated roles in coordinating the increased movement and thermogenesis that accompany the sexually receptive period in female mice[16,46]. Indeed, partial ablation of *Esr1*^{+} neurons in the VMH impairs BAT thermogenesis in females[9]. Additionally, activation of neurons in the VMHvl increases physical activity in females, but not in males, in a manner that is dependent on both circulating estrogens and hypothalamic expression of ERα[17]. Here, we find that specific activation of *Esr1*^{+} neurons in female VMHvl increases physical activity and body temperature, supporting the notion that *Esr1*^{+} VMHvl neurons coordinate estrogen-dependent energy expenditure.

The present results suggest that sex hormone signaling during development drives the emergence of two female-specific subpopulations of *Esr1*^{+} neurons, defined by largely mutually exclusive expression of either *Tac1* or *Rprm*. Previous studies link the *Tac1*^{+} subset of ERα^{+} neurons to the regulation of physical activity in females, without affecting thermogenesis[17]. To date, several lines of evidence have also implicated estrogen signaling in the VMH, primarily dependent on inhibition of AMP-kinase (AMPK), in enhanced BAT thermogenesis through activation of the sympathetic nervous system (SNS)[16,47]. We now report that silencing *Rprm* function selectively alters temperature without significantly affecting movement. Together, our expression analyses and functional studies suggest a model in which estrogens act on the *Tac1* and *Rprm* neuron clusters to increase energy expenditure in females by two distinct mechanisms (Figure 7e). The intermingling of *Tac1*^{+} and *Rprm*^{+} neurons within the VMHvl is intriguing. In the future, it will be very interesting to examine whether *Rprm*^{+} neurons and *Tac1*^{+} neurons exhibit crosstalk and how their circuit wiring differs, but this will require currently unavailable tools, such

27

as a *Rprm-Cre* mouse, to allow for specific labeling, activation, and inhibition of these populations.

These studies also uncovered a male-specific pattern of expression in the VMHvl, defined by the expression of *Pdyn*. A notable difference between the *Pdyn* and *Tac1* or *Rprm* subpopulations is that maintenance of *Pdyn* in the VMHvl expression requires circulating testicular hormones. This result is made more striking by the observation that *Pdyn* expression in the dorsomedial VMH (VMHdm) is contrastingly unaffected by castration. Dynorphins, the products of *Pdyn*, are potent endogenous opioid peptides[48] with demonstrated roles in reward, addiction, and stress[49]. It will be very interesting in future studies to examine the role of VMH *Pdyn* expression in male behavior, and how these behaviors might be modified by circulating levels of testosterone. In addition to the observed sub-specialization of the VMHvl, we observed a limited number of VMH-wide sex differences in gene expression, including male-biased expression of *Ndn*, which appears to be due to fewer Ndn^+ cells in the VMH of females compared to males.

Entry into menopause is associated with significant increases in visceral abdominal fat and body weight. Surprisingly, this is not associated with an increase in caloric intake. Instead, adiposity correlates with a decrease in overall energy expenditure, which manifests most strikingly during sleep[1], implying that an increasingly sedentary lifestyle cannot be the primary determinant. Because postmenopausal obesity confers enhanced risks of cardiovascular disease and breast cancer, there is a clear and urgent need to find new strategies to combat weight gain. Replacing hormones lost during menopause, such as estrogen and progesterone, can bring about weight loss, but these treatments themselves carry potential cardiovascular and cancer risks. We speculate that $Tac1^+$ and $Rprm^+$ neurons are important nodes in the dysregulation of energy expenditure accompanying the abrupt decline in circulating sex hormones experienced during menopause. As such, the molecular mechanism whereby these neurons control thermogenesis will be of interest for the treatment of post-menopausal obesity.

Experimental Procedures

Mice

All studies were carried out in accordance with the recommendations in the Guide for the Care and Use of Laboratory Animals of the National Institutes of Health. UCLA is AALAS accredited and the UCLA Institutional Animal Care and Use Committee (IACUC) approved all animal procedures. Mice expressing the *Sf1Cre* driver transgene (*Tg(Nr5a1-cre)7Lowl*), the *Nkx2-1Cre* driver transgene (*Tg(Nkx2-1-cre)2Sand*), and the *Ai14*-tdTomato reporter with loxP-flanked STOP cassette (*Gt(ROSA)26Sort^{m14(CAG-tdTomato)Hze}*) were maintained on a C57BL/6 genetic background. The *Esr1 floxed* allele (*Esr1^{tm1Sakh}*) was maintained on a CD-1;129P2 mixed background. Breeder male "Four Core Genotypes" mice (FCG, background C57BL/6J) possess a Y chromosome deleted for the testis-determining gene *Sry*, and an *Sry* transgene inserted into chromosome 3. The four genotypes include XX and XY gonadal males (XXM and XYM), and XX and XY gonadal females (XXF and XYF). Genotypes were discriminated using genomic PCR as described in [50]. All other experiments were carried out on C57BL/6J mice (JAX 000664). Except for gonadectomy studies, all experiments were performed in intact males and intact cycling females.

scRNA sequencing

We labeled all VMH neurons by crossing the Cre-dependent tdTomato reporter (*Ai14*)[30] to the *Sf1Cre* driver[29] to generate *Ai14^{f/f}; Sf1Cre* mice. Because the tdTomato signal is largely restricted to the VMH, a fairly large hypothalamic region was collected under fluorescent illumination. Cells were dissociated using a papain-based enzymatic process (Worthington Biochemical). VMH neurons were sorted by FACS using parameters that select for tdTomato signal. Because tdTomato is expressed in processes and projections, we enriched for cell bodies using a nuclear DNA dye (cell permeant DRAQ5, ThermoFisher). Dead cells were excluded by eliminating cells stained by NucBlue (cell impermeant DAPI). Doublet discrimination was used to

ensure single cells were deposited into each well. Individual tdTomato^{+} neurons were sorted into each well of a 96-well plate (Precise WTA kits, BD). The Precise WTA single cell sequencing kits include a well index to identify each cell and a unique molecular index (UMI) to identify each transcript and reduce bias due to PCR amplification. Libraries were prepared according to manufacturer's instructions and sequenced on an Illumina NextSeq 500 using paired end 2 x 75 bp mode.

Expression data were analyzed using the R package Seurat[51]. Normalized data were scaled with a linear regression model based on number of unique molecular identifiers (UMIs) per cell and percentage of reads from the mitochondrial genome to remove unwanted sources of variability and to normalize gene expression data. Analyses included all genes expressed in ≥ 2 cells, and all cells expressing ≥ 500 genes and a fraction of mitochondrial reads < 0.17. To cluster cells based on transcriptome similarity, we used Shared Nearest Neighbor (SNN) algorithm[52]. For each cell cluster, marker genes were determined by comparing expression in the given cluster against all other clusters using the smart local moving algorithm to iteratively group clusters together[52]. To determine sex differences, all female neurons passing initial filtering were compared to all male neurons passing initial filtering.

Mouse Procedures

Mice were anaesthetized with isofluorane and received analgesics (0.01mg/mL buprenorphine, 0.58mg/mL carprofen) pre- and post- surgery. Bilateral ovariectomy and castration surgery with complete removal of the ovaries or the testes was performed on adult mice. For Figure 4, sham or gonadectomized control mice (XXF and XYM) and gonadectomized FCG mice from separate experimental batches are shown together. The Cre-dependent AAV8-hM3Dq-mCherry DREADD (Addgene, titer ≥ 4×10^{12} vg/mL, 200 nL to each side) was injected bilaterally into the VMHvl of adult female mice (coordinates: A-P: -1.56 mm from Bregma; lateral: ±0.85 mm from Bregma; D-V: 5.6 mm from the cortex). After 2 weeks of recovery, mice received

i.p. injections of CNO (0.3 mg/kg) or vehicle (saline, 0.15% DMSO) 3 hr after the onset of the light phase. Saline and CNO were administered on consecutive days in a randomized balanced design. siRNA pools against *Rprm* or non-targeting controls (Dharmacon, 0.4 mM, 350 nL to each side) were delivered to the VMHvl as described above. Indirect calorimetry was performed in Oxymax metabolic chambers (Columbus Instruments). Gross movement and core body temperature were measured using an IP-implanted G2 eMitter and VitalView software (Starr Life Sciences).

RNA probe generation

Digoxigenin (DIG)- or fluorescein (FITC)-labeled sense and antisense riboprobes for somatostatin (*Sst),* reprimo (*Rprm),* tachykinin 1 (*Tac1),* prodynorphin (*Pdyn),* necdin (*Ndn),* and proto-oncogene, serine/threonine kinase A-Raf (*Araf)* were in vitro transcribed from template cDNA using T7/T3/SP6 RNA polymerase (DIG/FITC RNA labeling kit, Roche) and purified with RNA Clean & Concentrator (Zymo Research). For template cDNA generation, PCR products for individual genes were amplified from a hypothalamic cDNA library and cloned into pCR 2.1-TOPO or pCR II-TOPO (Invitrogen) for all probes except *Tac1*, which was previously described[17]. Plasmid DNA was isolated from bacterial cultures using ZymoPURE II Plasmid Midiprep kit (Zymo Research), linearized by restriction digest, and purified with DNA Clean & Concentrator (Zymo Research). All PCR products, except *Araf*, were generated using reference primer sequences from the Allen Brain Institute. For *Araf*, cDNA was generated from bases 639-942 (NM_009703.2).

In situ hybridization

The ISH protocol was partially adapted from previously published methods[17]. 18μm-thick cryosections containing the VMH were obtained from paraformaldehyde-fixed mouse brains. Day 1: Upon defrosting to room temperature (rt), slides were washed in PBS, postfixed in 4% PFA, and washed again. TSA-fluorescent ISH (FISH) slides were also incubated in 3% H_2O_2 for 30min to quench endogenous peroxidase activity. To permeabilize the tissues, slides were incubated in

31

proteinase K (1ug/mL) for TSA-FISH and chromogenic ISH (CISH), or 0.3% Triton X-100 in PBS for combined FISH-IHC. CISH slides were postfixed again in 4% PFA for 5 min. Slides were incubated in hyb solution containing probe overnight at 65C. Day 2: Coverslips were removed in solution containing 5x SSC heated to 65C. Slides were then subject to a series of stringency washes, then blocked in NTT containing 2% blocking reagent and HISS for 2 h at rt. Slides were incubated in antibody solution containing either anti-DIG-AP (1:5,000), anti-FITC-AP (1:5,000), or anti-DIG-POD (1:4,000) in 4C overnight. FISH-IHC slides were additionally incubated in anti-ERα (Rb, 1:1000). Day 3: Slides were washed in NTT, then NTTML (0.15M NaCl, 0.1M Tris pH 9.5, 50mM $MgCl_2$, 2mM levamisole, and 0.1% Tween-20) to quench endogenous phosphatase activity. Slides were developed in INT/BCIP solution (Roche). FISH-IHC slides were blocked in 10% normal goat serum for 1hr at rt, and incubated with anti-rabbit 647 for 2 h at rt, and incubated in HNPP/Fast red working solution according to manufacturer's instructions (HNPP Fluorescent Detection Set, Roche). To stop the reaction, the slides were washed 3x 5min in PBS, counterstained with DAPI, and immediately stored in -20C to prevent HNPP/Fastred diffusion. TSA-FISH slides were incubated in working solution containing Cy5 Plus tyramide according to manufacturer's instructions (Perkin Elmer). Slides were then washed in NTT and incubated in 3% H_2O_2 for 30min to quench the first tyramide reaction. Slides were then washed 3x 5min in NTT, blocked in in NTT containing 2% blocking reagent and HISS for 2 h at rt, and incubated overnight in anti-FITC-POD (1:4,000). Day 4: TSA-FISH slides were washed in NTT, and incubated in working solution containing FITC Plus tyramide according to manufacturer's instructions (Perkin Elmer). The reaction was terminated with NTT and slides were counterstained in DAPI. Control experiments using sense riboprobes and no probes showed negligible signal. Additionally, performing the TSA reaction following 3% H_2O_2 for 30min in the absence of a second POD incubation confirmed adequate quenching. Probes with weaker signal intensity were developed first in TSA-FISH.

Image Acquisition and Quantification

All CISH experiments with imaged in brightfield on a DM1000 LED microscope (Leica) using 5X or 10X objectives. Semi-quantitative optical density (O.D.) measurements of mRNA in CISH slides were obtained with ImageJ (NIH) following calibration with a calibrated step tablet (Kodak), according to standard protocols[53]. Measurements from the left and right VMH were averaged to calculate the mean O.D. for each animal using predetermined ROIs based on the Franklin and Paxinos Mouse Brain Atlas. Sex differences in O.D. between the caudal VMH and caudal VMHvl were determined by two-way ANOVA with Bonferroni multiple-comparison correction. FISH and IHC experiments were imaged on a LSM780 confocal microscope (Zeiss) using 10X or 20X objectives. Tile-scanned images were stitched using Zen Black (Zeiss). All images were taken with the same z-sampling interval for a given objective and z-stacks were merged to obtain maximum intensity projections. Cyan/magenta/yellow pseudo-colors were applied to all fluorescent images for accessibility. Image processing, limited to brightness and contrast, was performed using the Leica Application Suite (Leica), Zen Black (Zeiss), ImageJ (NIH), and Photoshop (Adobe).
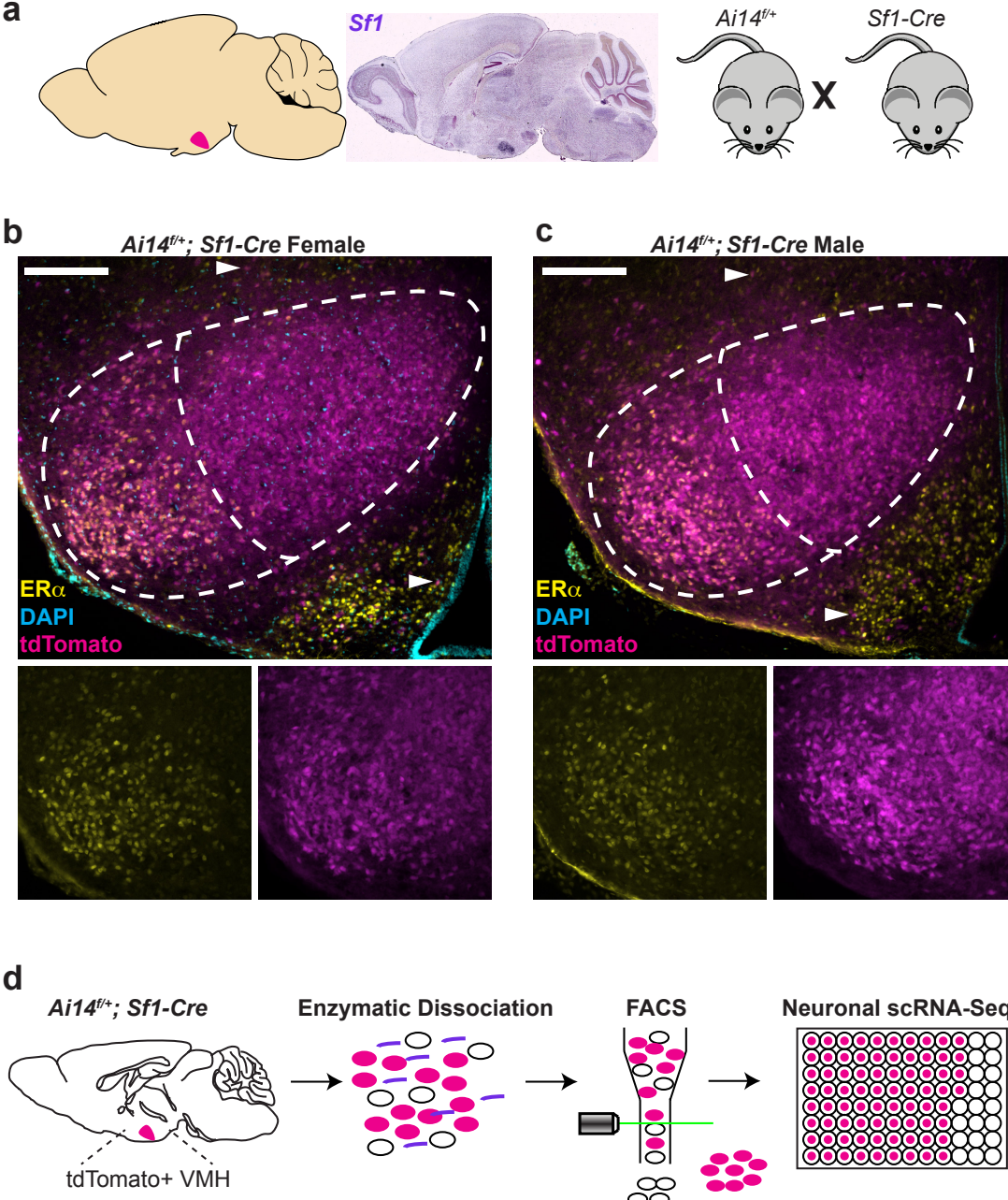
Acknowledgements

Author Contributions

JEV, LGK, and SMC conceived of and designed the studies. JEV, LGK, PCB, MS, MSR, JWP, ZZ, MGM, HH, and SMC acquired and analyzed data. JEV, LGK, PCB, MS, DA, ML, APA, XY, and SMC contributed to data interpretation. JEV, LGK, and SMC wrote the manuscript with substantial input from MS, ZZ, MGM, DA, ML, APA, and XY.

Competing Interests Statement

The authors declare no competing interests.

van Veen, Kammel, et al. Fig. 1
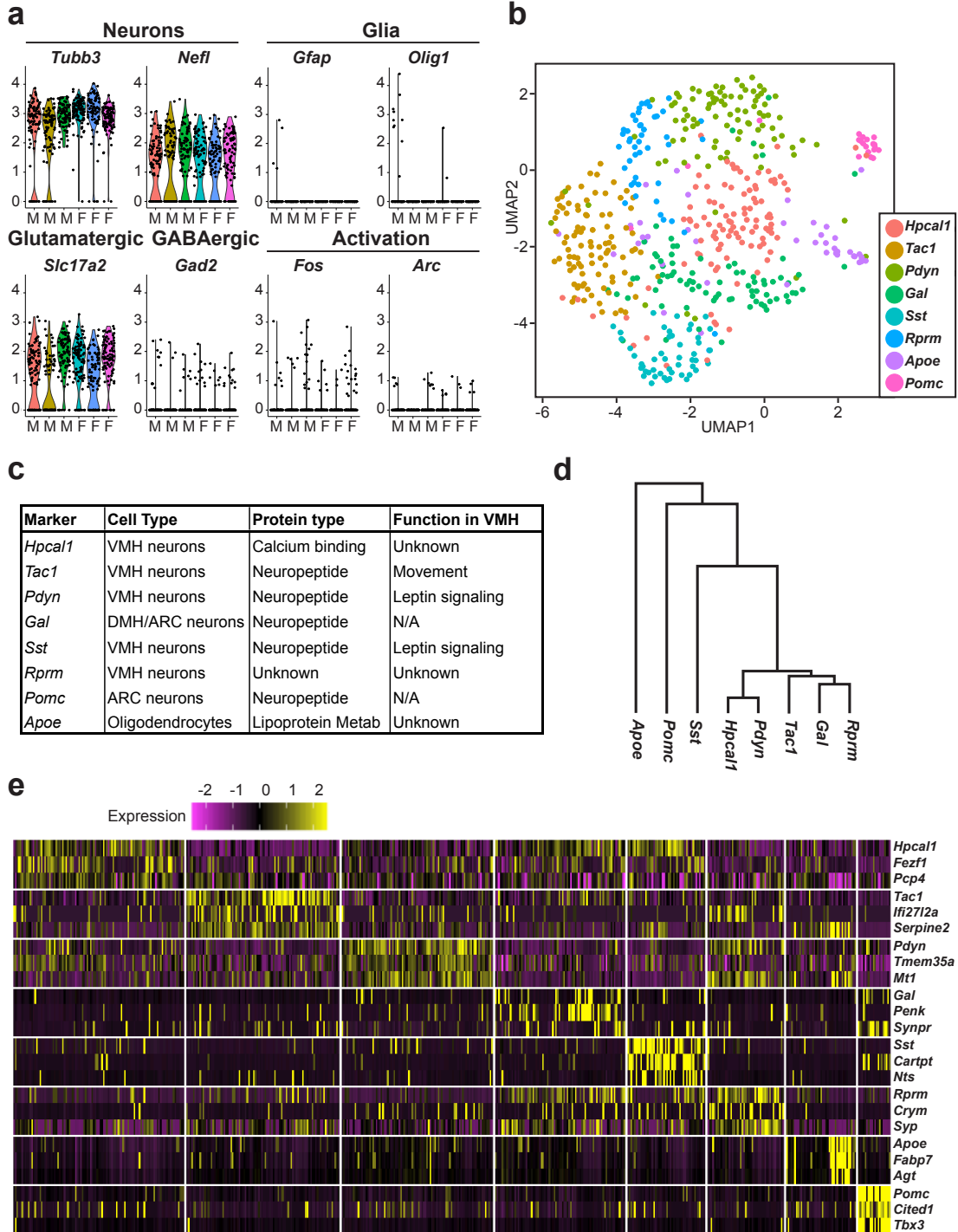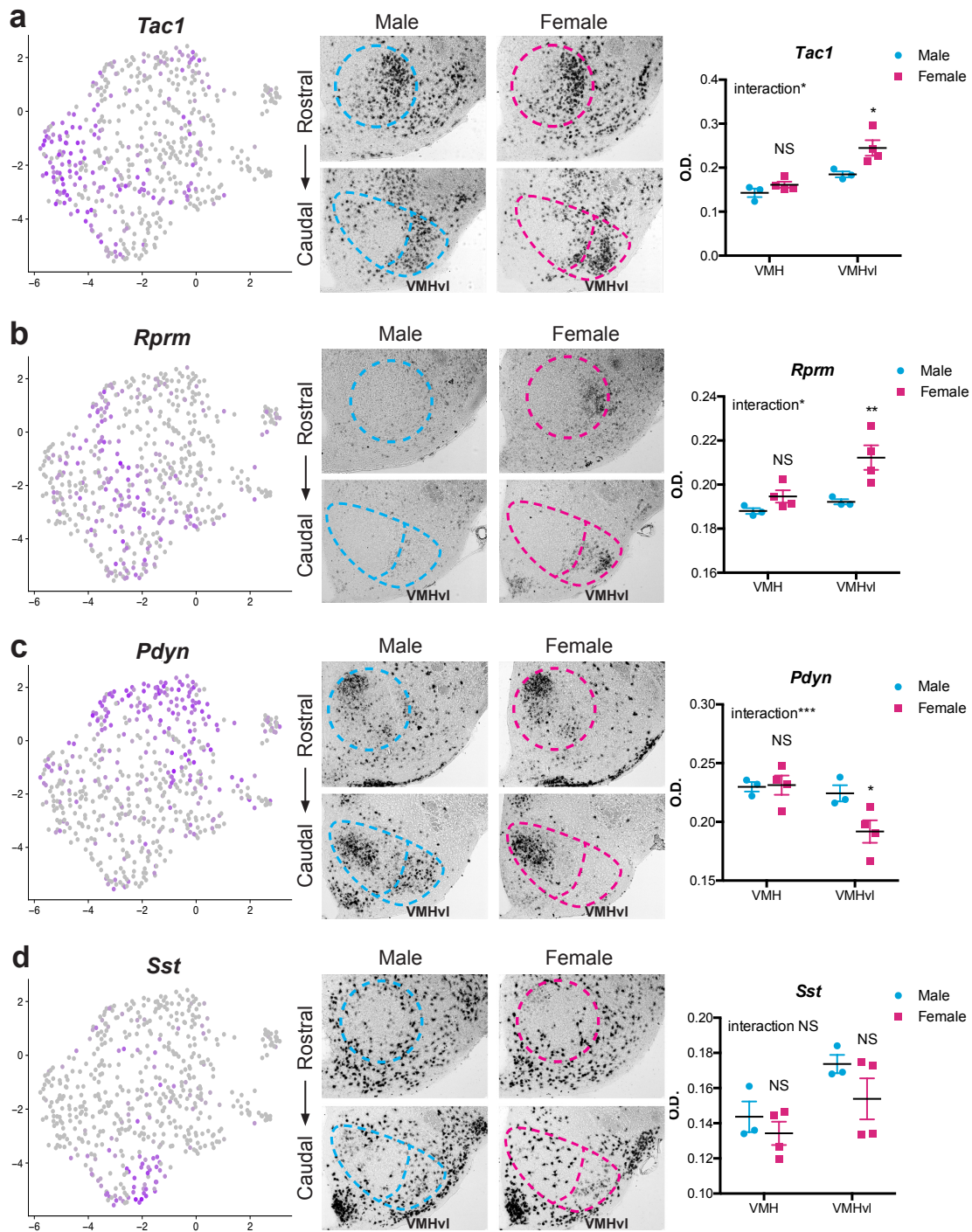
a

Sf1

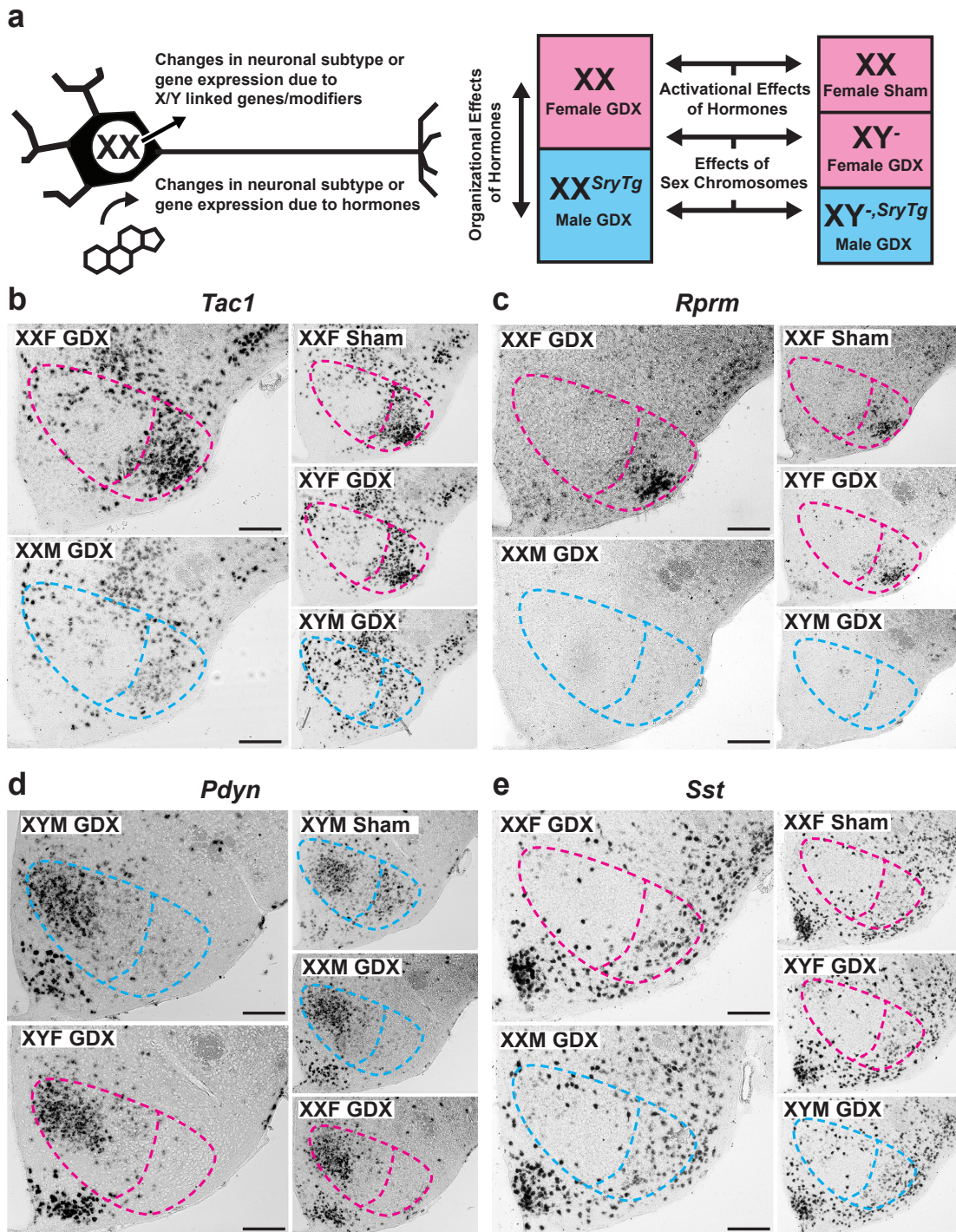*Ai14^{f/+}*   *Sf1-Cre*

X

b *Ai14^{f/+}; Sf1-Cre* Female

ERα
DAPI
tdTomato

c *Ai14^{f/+}; Sf1-Cre* Male

ERα
DAPI
tdTomato

d

Ai14^{f/+}; Sf1-Cre   **Enzymatic Dissociation**   **FACS**   **Neuronal scRNA-Seq**

tdTomato+ VMH

a

b

c

Marker	Cell Type	Protein type	Function in VMH
Hpcal1	VMH neurons	Calcium binding	Unknown
Tac1	VMH neurons	Neuropeptide	Movement
Pdyn	VMH neurons	Neuropeptide	Leptin signaling
Gal	DMH/ARC neurons	Neuropeptide	N/A
Sst	VMH neurons	Neuropeptide	Leptin signaling
Rprm	VMH neurons	Unknown	Unknown
Pomc	ARC neurons	Neuropeptide	N/A
Apoe	Oligodendrocytes	Lipoprotein Metab	Unknown

d

e

a

b *Tac1*

c *Rprm*

d *Pdyn*

e *Sst*

a

CRE dependent
Gq-DREADD

b

c

AAV-DIO-hM3Dq-mCherry

Esr1Cre

Wild-Type

d
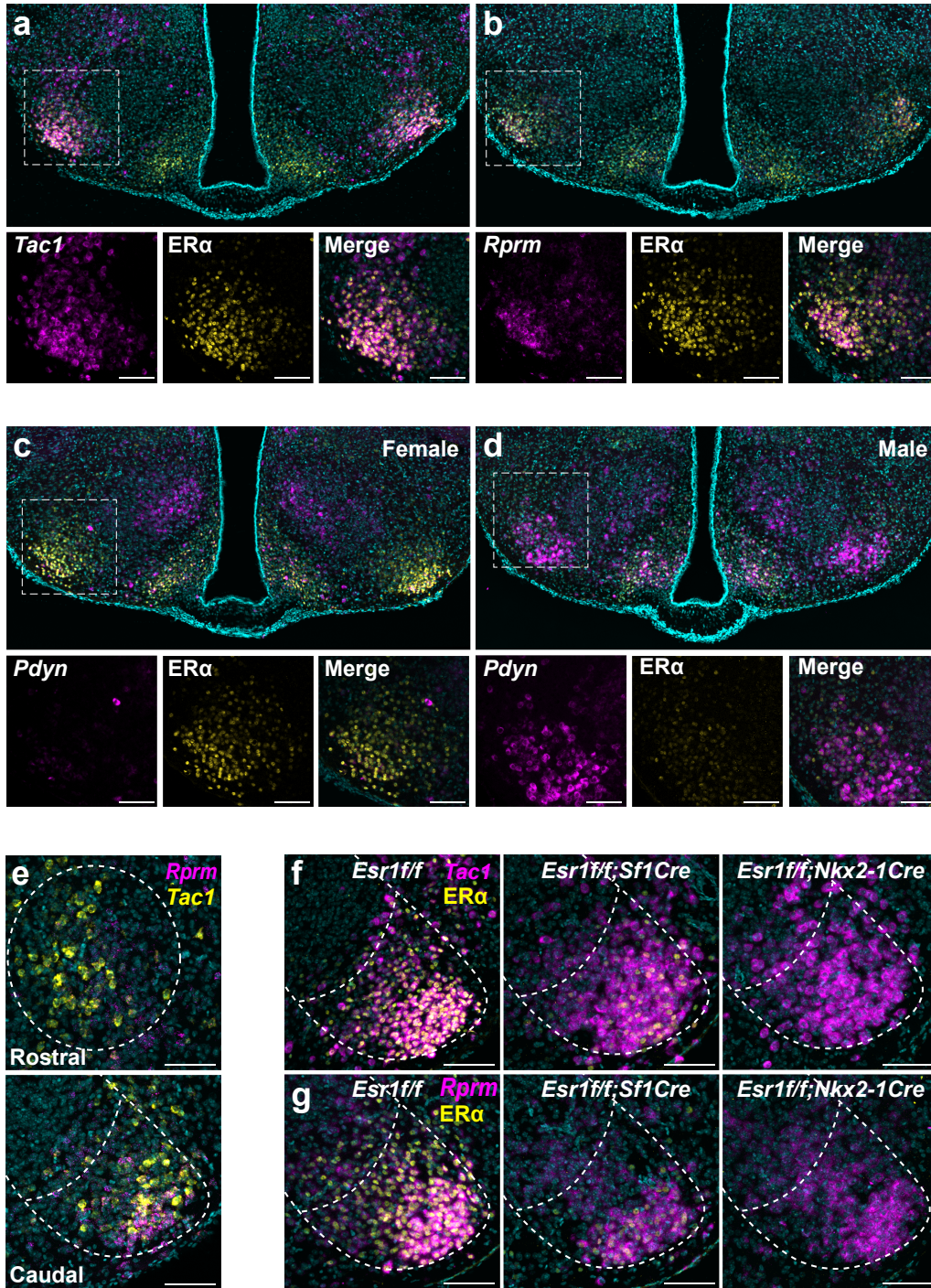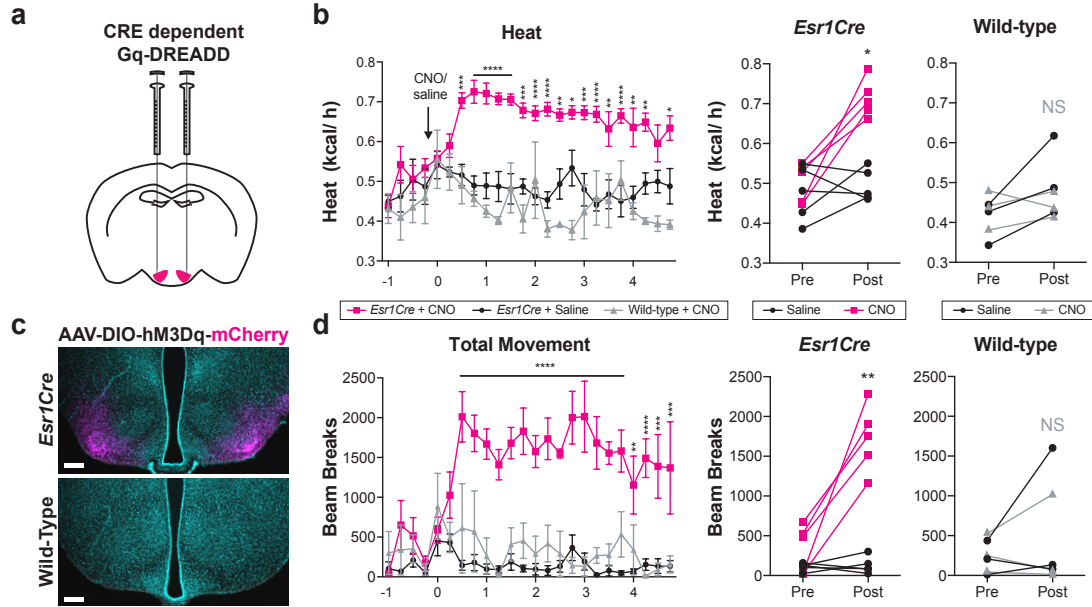
Figure Legends

Figure 1. *Sf1* **lineage tracing allows for targeted scRNA-seq of the VMH.**

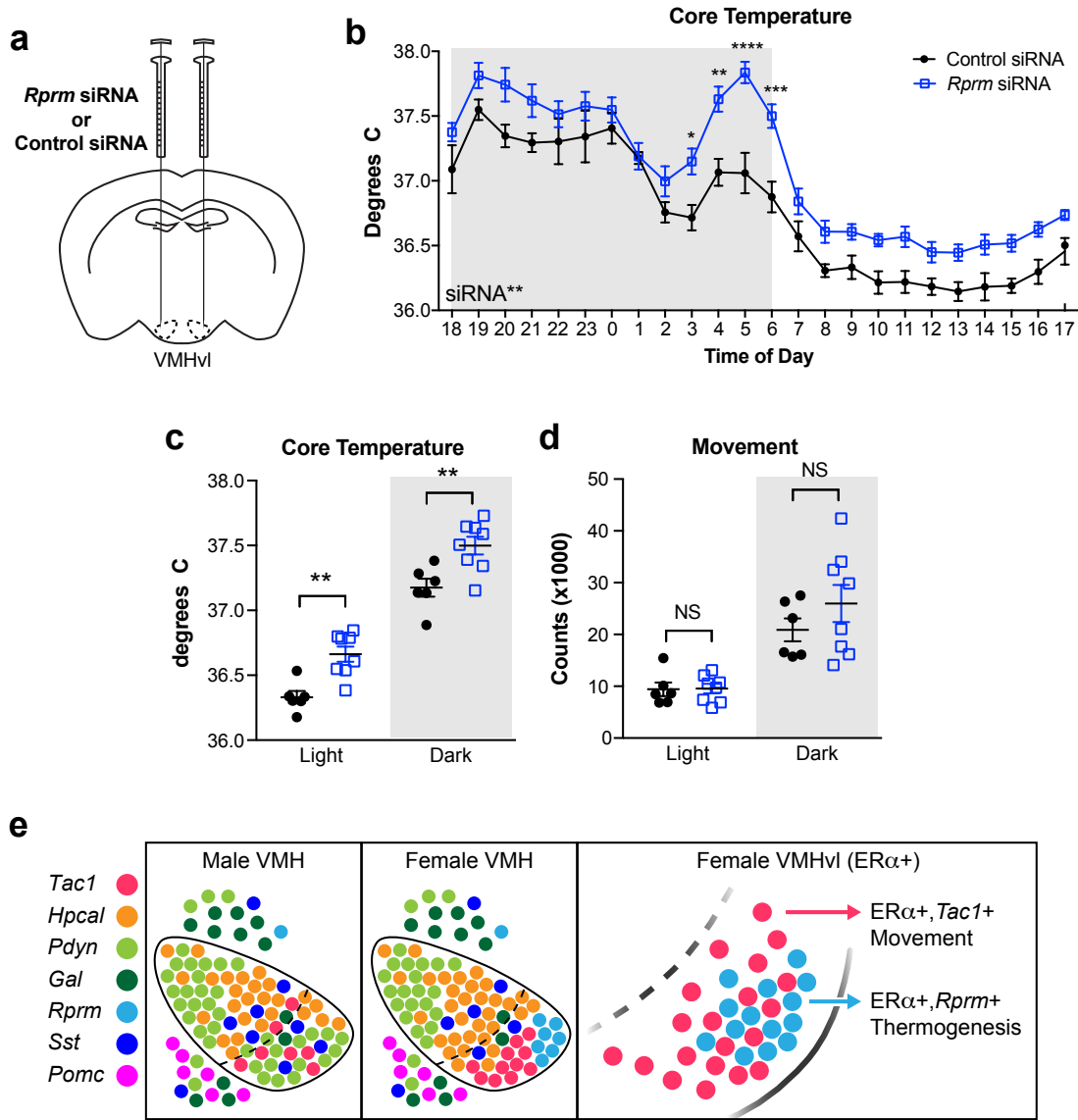**a,** In-situ hybridization of *Sf1* transcripts in sagittal section of mouse brain (from Allen Brain Atlas) shows a pattern of expression restricted to the VMH. **b,c,** Mice harboring both the *Sf1-Cre* allele and a latent allele of tdTomato (*Ai14*) show VMH specific fluorescence within the hypothalamus: coronal sections taken from P10 mice, scale bars = 200um. Both female (b) and male (c) VMH show expression of ERα in the VMHvl. As expected, females show higher immunoreactivity. White arrowheads highlight scattered *Sf1* lineage cells outside of the VMH. **d,** Strategy for dissociation followed by FACS and VMH targeted scRNA-seq.

Figure 2. Single cell RNA sequencing reveals non-overlapping gene expression signatures in the VMH.

a, scRNA sequencing results from (n = 3 female, 3 male) P10 mice showing high expression levels of the neuron specific markers *Tubb3* and *Nefl* with only scattered cells expressing the glial markers *Gfap* and *Olig1*. Cells also express high levels of the glutamatergic marker *Slc17a2*, low levels of the GABAergic marker *Gad2*, and limited expression of the immediate early genes *Fos* and *Arc*. **b,** UMAP showing clusters as defined by marker with highest expression relative to other clusters. **c,** Table showing predicted localization, protein type, and known function of cluster-defining markers. **d,** Hierarchical clustering tree showing relatedness of clusters based on transcriptional signatures. **e,** Heatmap showing expression of top three differentially expressed markers for each cluster.

Figure 3. *Tac1*, *Rprm*, **and** *Pdyn* **are sexually dimorphic genes in the adult VMHvl.** Spatial organization of cluster marker within the VMH. Cells positive for **a,** *Tac1*, **b,** *Rprm*, **c,** *Pdyn*, and

d, *Sst* are identified in purple within the UMAP (left panels). Spatial localization of each cluster marker along the rostral-caudal axis of the VMH in intact males (n = 3 mice) and females (n = 3-4 mice) by chromogenic ISH (right panels). mRNA levels were quantified within the caudal VMH and caudal VMHvl subregion. A statistically significant interaction between sex and ROI was determined for *Tac1* ($F_{(1,5)} = 8.932$, $p = 0.0305$), *Rprm* ($F_{(1,5)} = 13.23$, $p = 0.0149$), and *Pdyn* ($F_{(1,5)} = 65.84$, $p = 0.0005$). Post-hoc Sidak's multiple comparison tests revealed statistically significant sex differences in expression in the caudal VMHvl (*p = 0.0125 for Tac1, p = 0.0071 for Rprm, p = 0.0362 for Pdyn*). Dashed line shows boundary of VMH and VMHvl, in blue for male and magenta for female. Scalebars = 200µm, * = p<0.05, ** = p<0.01, *** = p<0.001.

Figure 4. Organizational effects of hormones establish sexual dimorphic expression of cluster markers. a, The Four-Core Genotypes (FCG) mouse model, which produces littermates of XX gonadal females (XXF), XX gonadal males (XXM) with an autosomal transgene of the testis-determining gene *Sry* (*Sry Tg*), XY gonadal males (XYM), and XY gonadal females (XYF) with the *Sry Tg*, can be used to determine if the origin of sexually dimorphic gene expression arises due to organizational effects of hormones, activational effects of hormones, or effects due to differences in sex chromosome complement. Expression of **b,** *Tac1*, **c,** *Rprm*, **d,** *Pdyn*, and **e,** *Sst* in the caudal VMH of gonadectomized (GDX) or sham FCG mice (n= 2-3 mice per group) by chromogenic ISH. Dashed line shows boundary of VMH and VMHvl, in blue for male and magenta for female. Scalebars = 200µm.

Figure 5. *Tac1*^{+} and *Rprm*^{+} cells are principal ERα-expressing neurons in the female VMHvl. Transcript expression (magenta) of **a,** *Tac1*, and **b,** *Rprm* is shown together with ERα immunoreactivity (yellow) in the VMHvl using fluorescent ISH (FISH, n = 5 female mice). Scalebars on insets = 100µm. Transcript expression of *Pdyn* (magenta) in the VMHvl of **c,** female mice (n = 5) and **d,** male mice (n = 5) and ERα immunoreactivity (yellow) using FISH/IHC.

Scalebars on insets = 100μm. **e,** *Rprm* (magenta) and *Tac1* (yellow) transcript expression is visualized using TSA-FISH (n = 5 female mice) in the rostral (top panel) and caudal (bottom panel) VMH. Scalebars = 100μm. Transcript expression (magenta) of **f,** *Tac1* and **g,** *Rprm* together with ERα immunoreactivity (yellow) is visualized in *Esr1^{f/f}* mice (n = 6 female mice, left panel), and mice with genetic ablation of ERα in neurons of *Sf1* lineage (*Esr1^{f/f};Sf1Cre*, n = 4 female mice, middle panel) and in neurons of *Nkx2-1* lineage (*Esr1^{f/f};Nkx2-1Cre*, n = 3 mice, right panel). Scalebars = 100μm. Images are merged with DAPI (cyan).

Figure 6. Specific activation of *Esr1^+* neurons in the VMHvl causes enhanced movement and thermogenesis

a,c, Strategy for and validation of stereotaxic injection of AAVs harboring CRE dependent Gq-coupled DREADDs in the VMHvl **b,** Heat generation increases acutely in *Esr1-Cre* animals after CNO injection but not after saline injection (n = 5 females). Two way RM ANOVA: Time (*F(23,92) = 4.542, p < 0.0001)*, CNO *(F(1,4) = 57.19, p = 0.0016)*, Interaction *(F(23,92) = 3.517, p < 0016)*. Wild-type littermate controls stereotaxically injected with the CRE dependent Gq-coupled DREADD show no significant increase in thermogenesis after CNO treatment (n = 3). **d,** Movement increases acutely in *Esr1-Cre* animals after CNO injection but not after saline injection. Two way RM ANOVA: Time (*F(23,92) = 6.361, p < 0.0001)*, CNO *(F(1,4) = 47.17, p = 0.0024)*, Interaction *(F(23,92) = 4.945, p < 0001)*. Wild-type animals stereotaxically injected with the CRE dependent Gq-coupled DREADD show no significant increase in movement after CNO treatment. Within-subject changes in average heat and average total movement are shown as averages 0-60 minutes prior to (Pre) and 30-90 minutes following the disturbance to deliver CNO (Post). All subjects were female wild-type mice, ages 10-18 weeks, and singly housed in indirect calorimetry chambers. Posthoc Sidak's multiple comparison tests were used for pairwise comparisons: * = p<0.05, ** = p<0.01, *** = p<0.001, **** = p<0.0001.

Figure 7. Temperature is dysregulated in mice lacking *Rprm*

a, Strategy for stereotaxic injection of cell-permeable siRNA pools either targeting *Rprm* (n = 6) or non-targeting (n = 8). **b,** Core temperature is significantly increased in animals injected with *Rprm* targeting siRNA pools compared to animals injected with non-targeting siRNA pools. Two way RM ANOVA: Interaction (*F(23,276) = 1.653, p = 0.0329)*, Time *(F(23,276) = 67.31, p <0.0001)*, siRNA *(F(1, 12) = 18.31, p = 0011)*. **c,** The effect of *Rprm* depletion on core temperature is significant in both the sleep (day) phase and active (night) phase compared to non-targeting controls. Two way RM ANOVA: Interaction (*F(1,12) = 1.653, p = 0.9408)*, Time *(F(1,12) = 330.1, p <0.0001)*, siRNA *(F(1, 12) = 18.31, p = 0011)*. **d,** *Rprm* depletion showed no significant effect on movement in either sleep or active phase when compared to non-targeting controls. All subjects were female wild-type mice, ages 10-20 weeks, and singly housed. **e,** diagram of neuronal populations found in the VMH with focus on sexually dimorphic female VMHvl. Posthoc Sidak's multiple comparison tests were used for pairwise comparisons: * = p<0.05, ** = p<0.01, *** = p<0.001, **** = p<0.0001.

Supplementary Figures:

Supplementary Figure 1. The overall architecture of the VMH is conserved between males and females.

Supplementary Figure 2. Clustering and expression of non-specific markers and markers outside of the VMH.

Supplementary Figure 3. Sexually dimorphic expression of *Pdyn* in the VMHvl is not maintained by differences in ovarian sex hormone signaling in adulthood.

Supplementary Figure 4. *Sst*^{+} cells show limited ERα immunoreactivity in the female VMHvl.

Supplementary Figure 5. DREADD activation increases cFOS immunoreactivity.

a

b

c *Ndn*

d Female | Male — *Ndn*

e *Araf*

**f** Female | Male — *Araf*

g Female | Male — VMHvl — ERα, pMEK
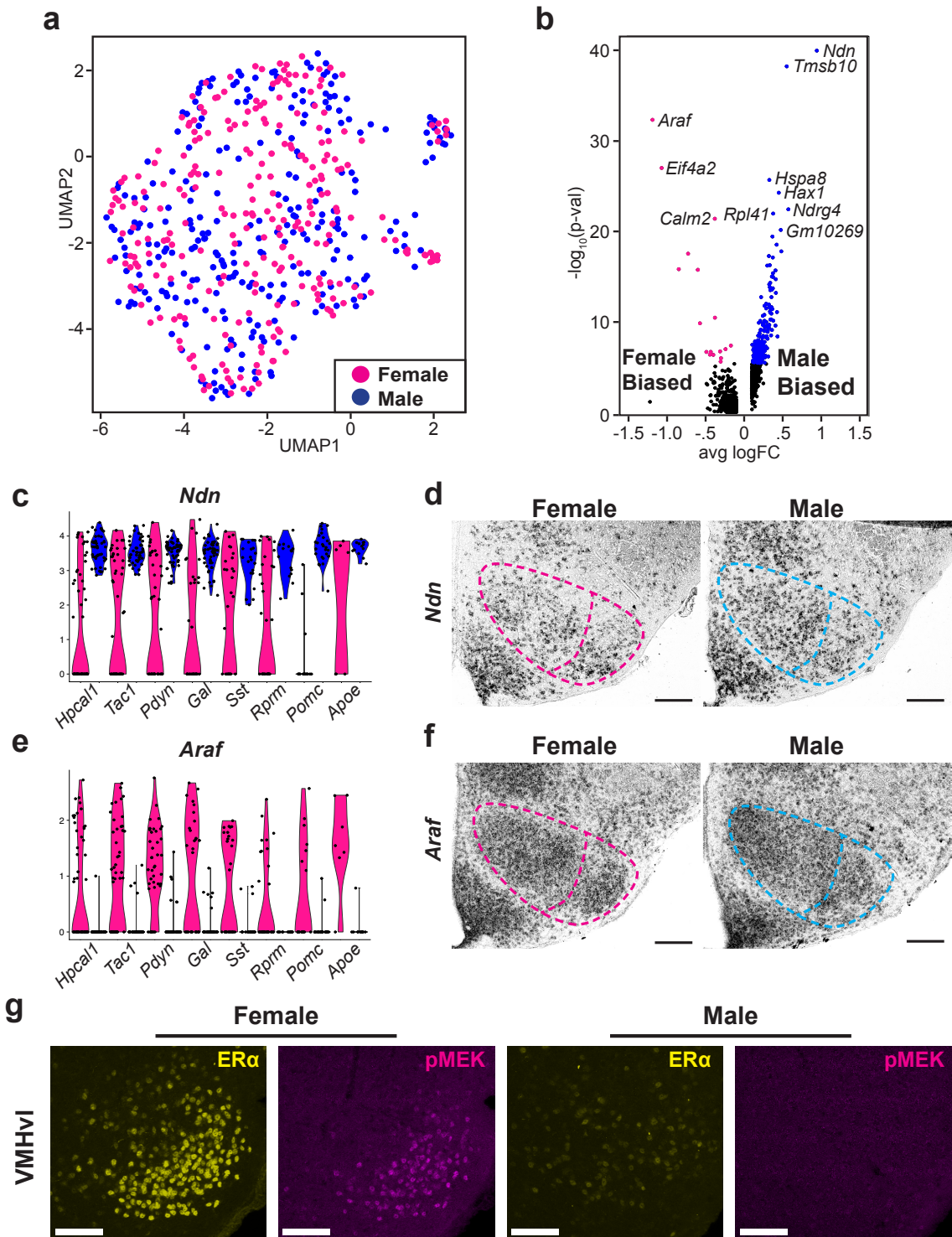
Supplementary Figure 1. The overall architecture of the VMH is conserved between males and females. Related to Figure 2. a, UMAP showing that male and female neurons are present in all clusters identified. **b,** Volcano plot showing differences in gene expression when comparing male and female VMH transcriptomes. Female biased (Adj. P < .05) genes shown in pink, male biased (Adj. P < .05) shown in blue. **c,** Violin plots showing male biased expression of *Ndn* across all VMH clusters. **d,** ISH validating male biased expression of *Ndn* in the VMH, scalebars = 200µm. **e,** Violin plots showing female biased expression of *Araf* across all clusters identified. **f,** ISH showing expression of *Araf* in male and female VMH, scalebars = 200µm. **g,** immunofluorescence demonstrating strong pMEK immunoreactivity in a subset of ERα expressing female neurons in the VMHvl, but no observable pMEK staining in the male VMHvl, scalebars = 100µm.
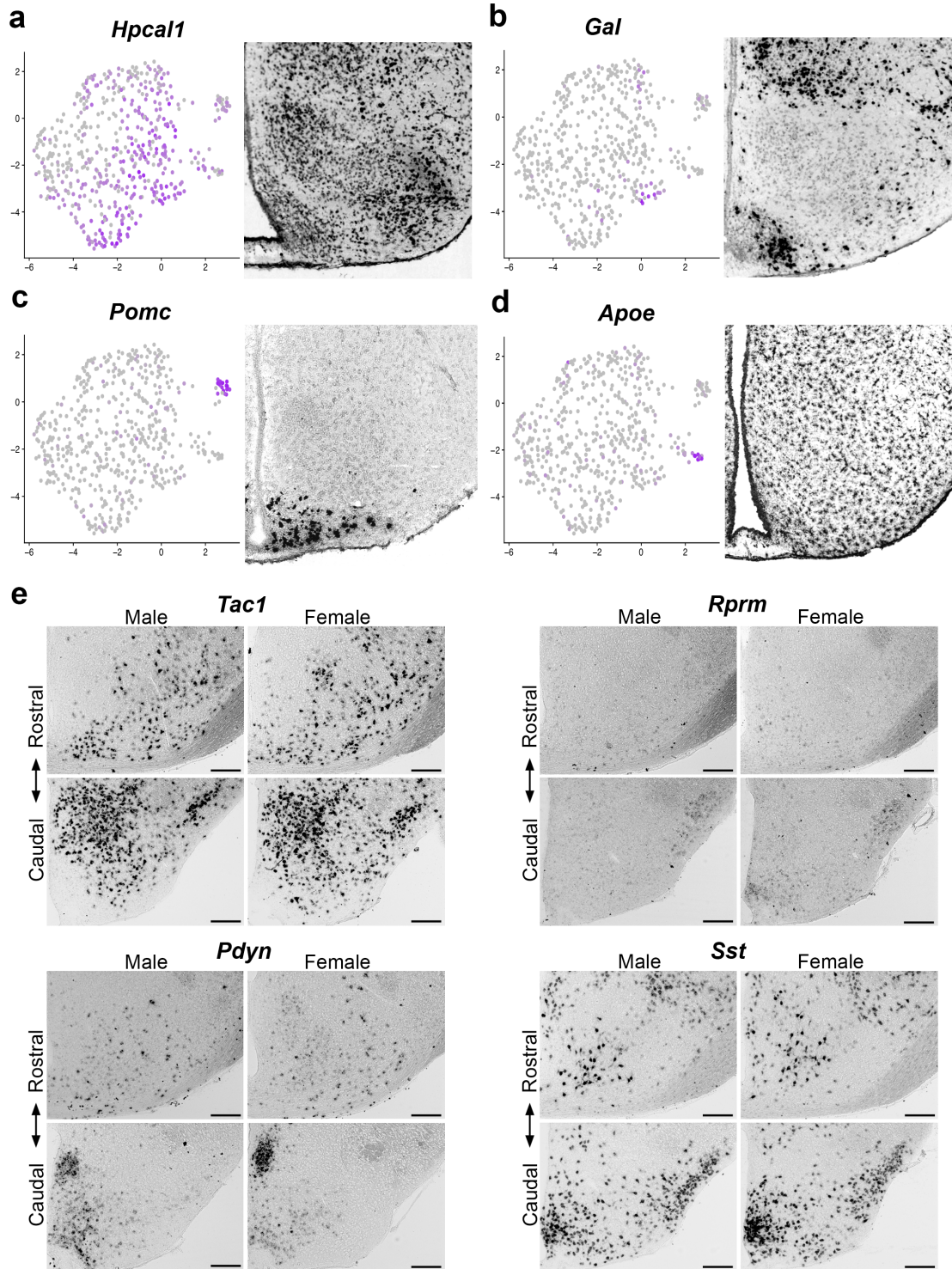
a *Hpcal1*

b *Gal*

c *Pomc*

d *Apoe*

e *Tac1*   *Rprm*

Pdyn   *Sst*

Supplementary Figure 2. Clustering and expression of non-specific markers and markers outside of the VMH. Related to Figure 3. a, *Hpcal1* expression appears diffusely in the UMAP clustering analysis, and similarly, ISH shows diffuse *Hpcal1* expression in the VMH. **b,** *Gal* expression is restricted to only a handful of cells on the UMAP, and similarly, ISH shows *Gal* expression in scattered VMH cells. **c,** *Pomc* expression is strongest outside of the central UMAP, and similarly, ISH shows *Pomc* expression strongest in the ARC. **d,** *Apoe* expression is strongest outside of the central UMAP. ISH shows *Apoe* expression with no particular pattern. **e,** expression of *Tac1*, *Rprm*, *Pdyn*, and *Sst* in brain areas adjacent to the VMH along the rostral-caudal axis in males (n=3) and females (n=4). Scalebars = 200µm. Images in **a-d** from Allen Brain Atlas.
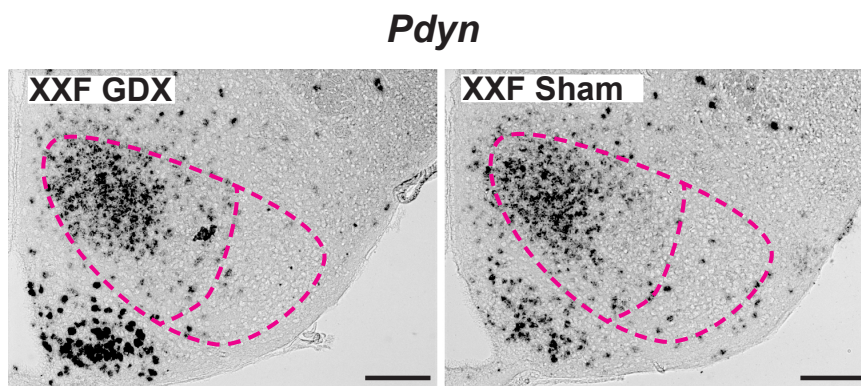
Pdyn

Supplementary Figure 3. Sexually dimorphic expression of *Pdyn* in the VMHvl is not maintained by differences in ovarian sex hormone signaling in adulthood. Related to Figure 4. Expression of *Pdyn* in the caudal VMH of gonadectomized (GDX) or sham XXF FCG mice (n=3 mice) by chromogenic ISH. Dashed line shows boundary of VMH and VMHvl, in magenta. Scalebars = 200µm.
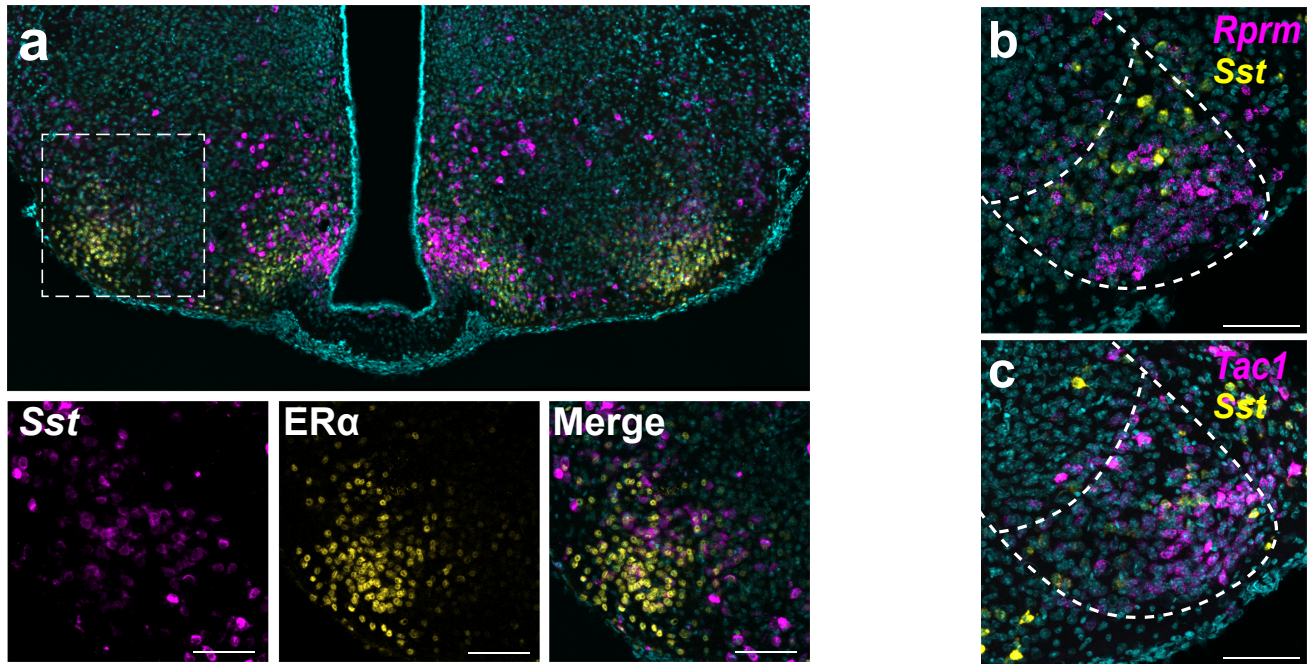
Supplementary Figure 4. *Sst*⁺ **cells show limited ERα immunoreactivity in the female VMHvl.**

Related to Figure 5. a, Transcript expression of *Sst* (magenta) is shown together with ERα immunoreactivity (yellow) in the VMHvl using fluorescent ISH (FISH, n=5 female mice). Scalebars on insets = 100µm. Transcript expression (magenta) of **b,** *Rprm,* and **c,** *Tac1* is visualized with *Sst* transcript expression (yellow) using TSA-FISH (n=5 female mice) in the caudal VMH. Scalebars = 100µm. Images are merged with DAPI (cyan).
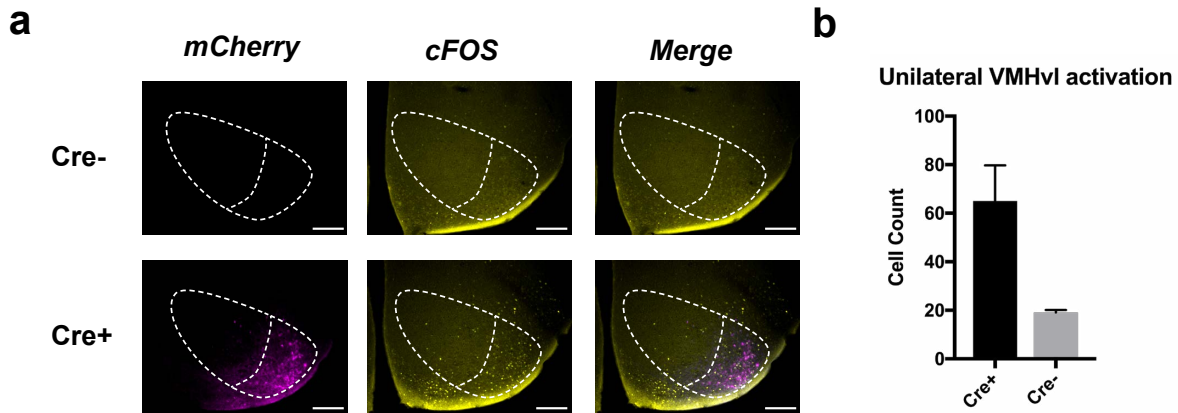
Supplementary Figure 5. DREADD activation increases cFOS immunoreactivity. Related to Figure 6. a, Representative images of increased mCherry (magenta) and cFOS (yellow) in the VMHvl of *Esr1Cre* (Cre+, n = 5) mice compared to wild-type (Cre-, n = 3) injected with a viral, cre-dependent mCherry-fused Gq-coupled DREADD. **b,** cFOS immunoreactivity in the VMHvl (quantified on one side per animal) is increased in Cre+ subjects 90 minutes following CNO injection. Scalebars = 200μm.

REFERENCES

1.   Lovejoy, J. C., Champagne, C. M., de Jonge, L., Xie, H. & Smith, S. R. Increased visceral fat and decreased energy expenditure during the menopausal transition. *Int J Obes (Lond)* **32**, 949–58 (2008).

2.   Slonaker, J. R. The effect of copulation, pregnancy, pseudopregnancy and lactation on the voluntary activity and food consumption of the albino rat. *Am J Physiol* **71**, (1925).

3.   Brobeck, J. R., Wheatland, M. & Strominger, J. L. Variations in regulation of energy exchange associated with estrus, diestrus and pseudopregnancy in rats. *Endocrinology* **40**, 65–72 (1947).

4.   Kopp, C., Ressel, V., Wigger, E. & Tobler, I. Influence of estrus cycle and ageing on activity patterns in two inbred mouse strains. *Behavioural brain research* **167**, 165–74 (2006).

5.   Olofsson, L. E., Pierce, A. A. & Xu, A. W. Functional requirement of AgRP and NPY neurons in ovarian cycle-dependent regulation of food intake. *Proceedings of the National Academy of Sciences of the United States of America* **106**, 15932–7 (2009).

6.   Sanchez-Alavez, M., Alboni, S. & Conti, B. Sex- and age-specific differences in core body temperature of C57Bl/6 mice. *Age (Dordr)* **33**, 89–99 (2011).

7.   Heine, P. A., Taylor, J. A., Iwamoto, G. A., Lubahn, D. B. & Cooke, P. S. Increased adipose tissue in male and female estrogen receptor-alpha knockout mice. *Proceedings of the National Academy of Sciences of the United States of America* **97**, 12729–34 (2000).

8.   Park, C. J. *et al.* Genetic rescue of nonclassical ERalpha signaling normalizes energy balance in obese Eralpha-null mutant mice. *The Journal of clinical investigation* **121**, 604–12 (2011).

9.   Xu, Y. *et al.* Distinct hypothalamic neurons mediate estrogenic effects on energy homeostasis and reproduction. *Cell metabolism* **14**, 453–65 (2011).

10.   Hulley, S. *et al.* Randomized Trial of Estrogen Plus Progestin for Secondary Prevention of Coronary Heart Disease in Postmenopausal Women. *JAMA* **280**, 605–613 (1998).

11.   Writing Group for the Women's Health Initiative Investigators. Risks and Benefits of Estrogen Plus Progestin in Healthy Postmenopausal WomenPrincipal Results From the Women's Health Initiative Randomized Controlled Trial. *JAMA* **288**, 321–333 (2002).

12.   Smith, A. W., Bosch, M. A., Wagner, E. J., Rønnekleiv, O. K. & Kelly, M. J. The membrane estrogen receptor ligand STX rapidly enhances GABAergic signaling in NPY/AgRP neurons: role in mediating the anorexigenic effects of 17β-estradiol. *American Journal of Physiology-Endocrinology and Metabolism* **305**, E632–E640 (2013).

13.   Ismael González-García *et al.* mTOR signaling in the arcuate nucleus of the hypothalamus mediates the anorectic action of estradiol. *Journal of Endocrinology* **238**, 177–186 (2018).

14.   Herber, C. B. *et al.* Estrogen signaling in arcuate Kiss1 neurons suppresses a sex-dependent female circuit promoting dense strong bones. *Nature Communications* **10**, 163 (2019).

15.   Musatov, S. *et al.* Silencing of estrogen receptor alpha in the ventromedial nucleus of hypothalamus leads to metabolic syndrome. *Proceedings of the National Academy of Sciences of the United States of America* **104**, 2501–6 (2007).

16.   Martinez de Morentin, P. B. *et al.* Estradiol Regulates Brown Adipose Tissue Thermogenesis via Hypothalamic AMPK. *Cell metabolism* **20**, 41–53 (2014).

17.   Correa, S. M. *et al.* An estrogen-responsive module in the ventromedial hypothalamus selectively drives sex-specific activity in females. *Cell Rep* **10**, 62–74 (2015).

18.   Hashikawa, K. *et al.* Esr1+ cells in the ventromedial hypothalamus control female aggression. *Nature Neuroscience* **20**, 1580 (2017).

19.   Lin, D. *et al.* Functional identification of an aggression locus in the mouse hypothalamus. *Nature* **470**, 221–6 (2011).

20.   Lee, H. *et al.* Scalable control of mounting and attack by Esr1+ neurons in the ventromedial hypothalamus. *Nature* **509**, 627–32 (2014).

21.   Yang, C. F. *et al.* Sexually dimorphic neurons in the ventromedial hypothalamus govern mating in both sexes and aggression in males. *Cell* **153**, 896–909 (2013).

22.   Wang, L. *et al.* Hypothalamic Control of Conspecific Self-Defense. *Cell Reports* **26**, 1747-1758.e5 (2019).

23.   Silva, B. A. *et al.* Independent hypothalamic circuits for social and predator fear. *Nature neuroscience* **16**, 1731–3 (2013).

24.   Remedios, R. *et al.* Social behaviour shapes hypothalamic neural ensemble representations of conspecific sex. *Nature* **550**, 388–392 (2017).

25.   Narita, K., Murata, T. & Matsuoka, S. The ventromedial hypothalamus oxytocin induces locomotor behavior regulated by estrogen. *Physiology & behavior* **164**, 107–12 (2016).

26.   Flanagan-Cato, L. M. Sex differences in the neural circuit that mediates female sexual receptivity. *Frontiers in neuroendocrinology* **32**, 124–36 (2011).

27.   Yang, T. & Shah, N. M. Molecular and neural control of sexually dimorphic social behaviors. *Curr Opin Neurobiol* **38**, 89–95 (2016).

28.   Krause, W. C. & Ingraham, H. A. Origins and Functions of the Ventrolateral VMH: A Complex Neuronal Cluster Orchestrating Sex Differences in Metabolism and Behavior. in *Sex and Gender Factors Affecting Metabolic Homeostasis, Diabetes and Obesity* (ed. Mauvais-Jarvis, F.) 199–213 (Springer International Publishing, 2017). doi:10.1007/978-3-319-70178-3_10

29.   Dhillon, H. *et al.* Leptin directly activates SF1 neurons in the VMH, and this action by leptin is required for normal body-weight homeostasis. *Neuron* **49**, 191–203 (2006).

30.   Madisen, L. *et al.* A robust and high-throughput Cre reporting and characterization system for the whole mouse brain. *Nature neuroscience* **13**, 133–40 (2010).

31.   Cheung, C. C., Kurrasch, D. M., Liang, J. K. & Ingraham, H. A. Genetic labeling of steroidogenic factor-1 (SF-1) neurons in mice reveals ventromedial nucleus of the hypothalamus (VMH) circuitry beginning at neurogenesis and development of a separate non-SF-1 neuronal cluster in the ventrolateral VMH. *J Comp Neurol* **521**, 1268–88 (2012).

32.   Sheng, M. & Greenberg, M. E. The regulation and function of c-fos and other immediate early genes in the nervous system. *Neuron* **4**, 477–485 (1990).

33.   Wu, Y. E., Pan, L., Zuo, Y., Li, X. & Hong, W. Detecting Activated Cell Populations Using Single-Cell RNA-Seq. *Neuron* **96**, 313-329.e6 (2017).

34.   McInnes, L., Healy, J. & Melville, J. UMAP: Uniform Manifold Approximation and Projection for Dimension Reduction. *arXiv:1802.03426v2*

35.   Malik, S. *et al.* Histone deacetylase 7 and FoxA1 in estrogen-mediated repression of RPRM. *Mol Cell Biol* **30**, 399–412 (2010).

36.   Allison, M. B. *et al.* TRAP-seq defines markers for novel populations of hypothalamic and brainstem LepRb neurons. *Molecular Metabolism* **4**, 299–309 (2015).

37.   Tannenbaum, G. S. & Bowers, C. Y. Interactions of growth hormone secretagogues and growth hormone-releasing hormone/somatostatin. *Endocrine* **14**, 21–27 (2001).

38.   Luo, S. X. *et al.* Regulation of feeding by somatostatin neurons in the tuberal nucleus. *Science* **361**, 76 (2018).

39.   Schick, R. R. *et al.* Effect of galanin on food intake in rats: involvement of lateral and ventromedial hypothalamic sites. *American Journal of Physiology-Regulatory, Integrative and Comparative Physiology* **264**, R355–R361 (1993).

40.   Arnold, A. P. & Chen, X. What does the 'four core genotypes' mouse model tell us about sex differences in the brain and other tissues? *Front Neuroendocrinol* **30**, 1–9 (2009).

41.   Dong, S., Allen, J. A., Farrell, M. & Roth, B. L. A chemical-genetic approach for precise spatio-temporal control of cellular signaling. *Molecular bioSystems* **6**, 1376–80 (2010).

42.   Chen, R., Wu, X., Jiang, L. & Zhang, Y. Single-Cell RNA-Seq Reveals Hypothalamic Cell Diversity. *Cell Rep* **18**, 3227–3241 (2017).

43.   Romanov, R. A. *et al.* Molecular interrogation of hypothalamic organization reveals distinct dopamine neuronal subtypes. *Nature Neuroscience* **20**, 176 (2016).

44.   Yang, C. F. & Shah, N. M. Representing sex in the brain, one module at a time. *Neuron* **82**, 261–78 (2014).

45.   McCarthy, M. M., Pickett, L. A., VanRyzin, J. W. & Kight, K. E. Surprising origins of sex differences in the brain. *Hormones and Behavior* **76**, 3–10 (2015).

46.   Clegg, D. J. *et al.* Estradiol-dependent decrease in the orexigenic potency of ghrelin in female rats. *Diabetes* **56**, 1051–8 (2007).

47.   Contreras, C. *et al.* The brain and brown fat. *Ann Med* **47**, 150–68 (2015).

48.   Chavkin, C., James, I. & Goldstein, A. Dynorphin is a specific endogenous ligand of the kappa opioid receptor. *Science* **215**, 413 (1982).

49.   Bruchas, M. R., Land, B. B. & Chavkin, C. The dynorphin/kappa opioid system as a modulator of stress-induced and pro-addictive behaviors. *Brain Research* **1314**, 44–55 (2010).

50.   Burgoyne, P. S. & Arnold, A. P. A primer on the use of mouse models for identifying direct sex chromosome effects that cause sex differences in non-gonadal tissues. *Biology of sex differences* **7**, 68–68 (2016).

51.   Satija, R., Farrell, J. A., Gennert, D., Schier, A. F. & Regev, A. Spatial reconstruction of single-cell gene expression data. *Nat Biotechnol* **33**, 495–502 (2015).

52.   Blondel, V. D., Guillaume, J.-L., Lambiotte, R. & Lefebvre, E. Fast unfolding of communities in large networks. *Journal of Statistical Mechanics: Theory and Experiment* **2008**, P10008 (2008).

53.   Robbins, E. *et al.* Quantitative non-radioactive in situ hybridization of preproenkephalin mRNA with digoxigenin-labeled cRNA probes. *Anat Rec* **231**, 559–62 (1991).